

# Dipolar Recoupling: Heteronuclear

Christopher P. Jaroniec

Ohio State University, Columbus, OH, USA

---

1	Introduction	1
2	MAS Hamiltonian	3
3	Heteronuclear Dipolar Recoupling in Spin Pairs	4
4	Heteronuclear Dipolar Recoupling in Multispin Systems	8
5	Conclusions	16
6	Related Articles	16
7	References	17

---

## 1 INTRODUCTION

Currently, high-resolution and high sensitivity NMR spectra of various types of polycrystalline solid samples containing low- $\gamma$  spin-1/2 nuclei, such as  $^{31}\text{P}$ ,  $^{13}\text{C}$ , and  $^{15}\text{N}$ , can be recorded on a relatively routine basis. This is made possible by the combined effects of (i) high static magnetic fields up to  $\sim 22$  T (950 MHz proton frequency), (ii) magic-angle spinning (MAS)<sup>1–3</sup> which involves the rapid rotation of the sample (at frequencies up to  $\sim 70$  kHz) about an axis tilted relative to the magnetic field at an angle  $\tan^{-1} \sqrt{2} \approx 54.74^\circ$  (see *Magic-Angle Spinning* and *Rotating Solids*), (iii) cross-polarization (CP) from protons<sup>4,5</sup> (see *Cross Polarization in Solids*), and (iv) efficient proton decoupling<sup>6–8</sup> (see *Heteronuclear Decoupling in Solids*). MAS facilitates the acquisition of high-resolution solid-state nuclear magnetic resonance (SSNMR) spectra by effectively averaging the anisotropic parts of nuclear spin interactions that can be represented by second-rank tensors<sup>9</sup>: chemical shifts and through-space dipole–dipole couplings for spin-1/2 systems (see *Internal Spin Interactions and Rotations in Solids*). Consequently, in order for these interactions – which are the primary source of information about three-dimensional molecular structure – to be detected and quantified under MAS conditions, they must be reintroduced or “recoupled” into the spectra. This type of recoupling can generally be achieved by the concurrent application of radiofrequency (RF) pulse sequences that appropriately manipulate the spin parts of the chemical shift and dipolar Hamiltonians and interfere with their spatial averaging due to MAS – note, however, that, in certain cases, purely MAS-driven recoupling is also possible.<sup>10–13</sup>

As thoroughly discussed elsewhere<sup>14–18</sup> (see *REDOR and TEDOR: Homonuclear Recoupling Schemes in MAS NMR*), beginning in the late 1980s, a number of major advances have been made in the development of MAS NMR pulse schemes designed to recouple homonuclear and heteronuclear dipolar interactions as well as chemical shift anisotropies (CSA), with most of the initial dipolar recoupling schemes geared toward isolated spin-1/2 pairs, such as  $^{13}\text{C}$ – $^{13}\text{C}$ ,  $^{13}\text{C}$ – $^{31}\text{P}$ , or  $^{13}\text{C}$ – $^{15}\text{N}$ , incorporated at specific sites in the sample by using various isotopic labeling approaches. Several of these

dipolar recoupling schemes including rotational echo double resonance (REDOR),<sup>19,20</sup> rotational resonance ( $R^2$ ),<sup>11,12</sup> and dipolar recoupling with a windowless sequence (DRAWS)<sup>21</sup> permit highly accurate and precise measurements of dipolar couplings as low as  $\sim 20$ – $30$  Hz to be performed. This yields quantitative, site-specific internuclear distance restraints up to  $\sim 6$ – $8$  Å (note that the range of accessible distances can be further increased to  $\sim 10$ – $15$  Å by using selective  $^{19}\text{F}$  labeling<sup>22</sup>) with uncertainties of a few tenths of an angstrom, and, as a result, these methods have had and continue to have tremendous impact on the SSNMR characterization of molecular structures of challenging biological systems<sup>15,22–25</sup> such as protein–protein and protein–ligand complexes,<sup>26–28</sup> membrane proteins,<sup>29–31</sup> surface-bound peptides,<sup>32</sup> and high-molecular-weight peptide and protein aggregates<sup>24,33–35</sup> (see *Rotational Resonance in Biology; Bacteriorhodopsin and Rhodopsin; Structure and Dynamics of Proteins Adsorbed at Biomaterial Interfaces*).

Notwithstanding the numerous successful applications of homonuclear and heteronuclear dipolar recoupling techniques to biological solids containing “magnetically dilute” spin-1/2 pairs, there is a compelling motivation for pursuing analogous types of experiments in highly or uniformly  $^{13}\text{C}$ ,  $^{15}\text{N}$  ( $\text{U-}^{13}\text{C}$ ,  $^{15}\text{N}$ ) labeled molecules. The primary advantage offered by multispin systems of this type is that a multitude of site-resolved structural restraints can, in principle, be extracted by using one or few samples, as is done routinely in the context of modern biomolecular solution-state NMR<sup>36,37</sup> (see *Biological Macromolecules: Structure Determination in Solution; Three- and Four-Dimensional Heteronuclear Magnetic Resonance*). Indeed, in recent years, by taking advantage of the principles of multidimensional spectroscopy<sup>38</sup> (see *Multidimensional Spectroscopy: Concepts*) and improved sample-preparation methods,<sup>39–42</sup> highly resolved MAS NMR spectra were reported for a number of  $\text{U-}^{13}\text{C}$ ,  $^{15}\text{N}$  enriched biological macromolecules, which paved the way for the detailed characterization of molecular structure and dynamics in these systems and demonstrated the general feasibility of such studies<sup>43–45</sup> (see *Structure Determination of Solid Proteins Using MAS and Isotopic Enrichment*). To illustrate the resolution and sensitivity of SSNMR spectra that can be obtained for  $\text{U-}^{13}\text{C}$ ,  $^{15}\text{N}$  labeled biological molecules of varying complexity at, by today’s standards, moderate magnetic fields ( $\omega_0/2\pi \sim 500$  MHz for protons) and MAS rates ( $\omega_r/2\pi \sim 10$  kHz), in Figure 1 we show 1-D  $^{13}\text{C}$  and  $^{15}\text{N}$  CP-MAS spectra of a three-residue peptide, formyl-Met-Leu-Phe (f-MLF),<sup>46,47</sup> and 2-D  $^{15}\text{N}$ – $^{13}\text{C}$  SPECIFIC-CP<sup>48</sup> correlation spectra of amyloid fibrils formed by residues 23–144 of human prion protein (huPrP23-144).<sup>49</sup>

In instances where the recoupling of nominally large, one-bond dipolar interactions (Table 1) is of interest, the original pulse schemes developed for selectively isotope labeled samples can often be applied directly to  $\text{U-}^{13}\text{C}$ ,  $^{15}\text{N}$  labeled ones with minimal or no modifications. Examples of such applications include magnetization transfer in multidimensional chemical shift correlation experiments,<sup>50,51</sup> characterization of conformational dynamics<sup>52–59</sup> (see *Double-Quantum NMR Spectroscopy of Dipolar Coupled Spins Under Fast Magic-angle Spinning; Dipolar Coupling: Molecular-Level Mobility*), and measurements of relative dipole tensor orientations, which yield protein backbone and side-chain dihedral angle restraints.<sup>60–74</sup> On the other

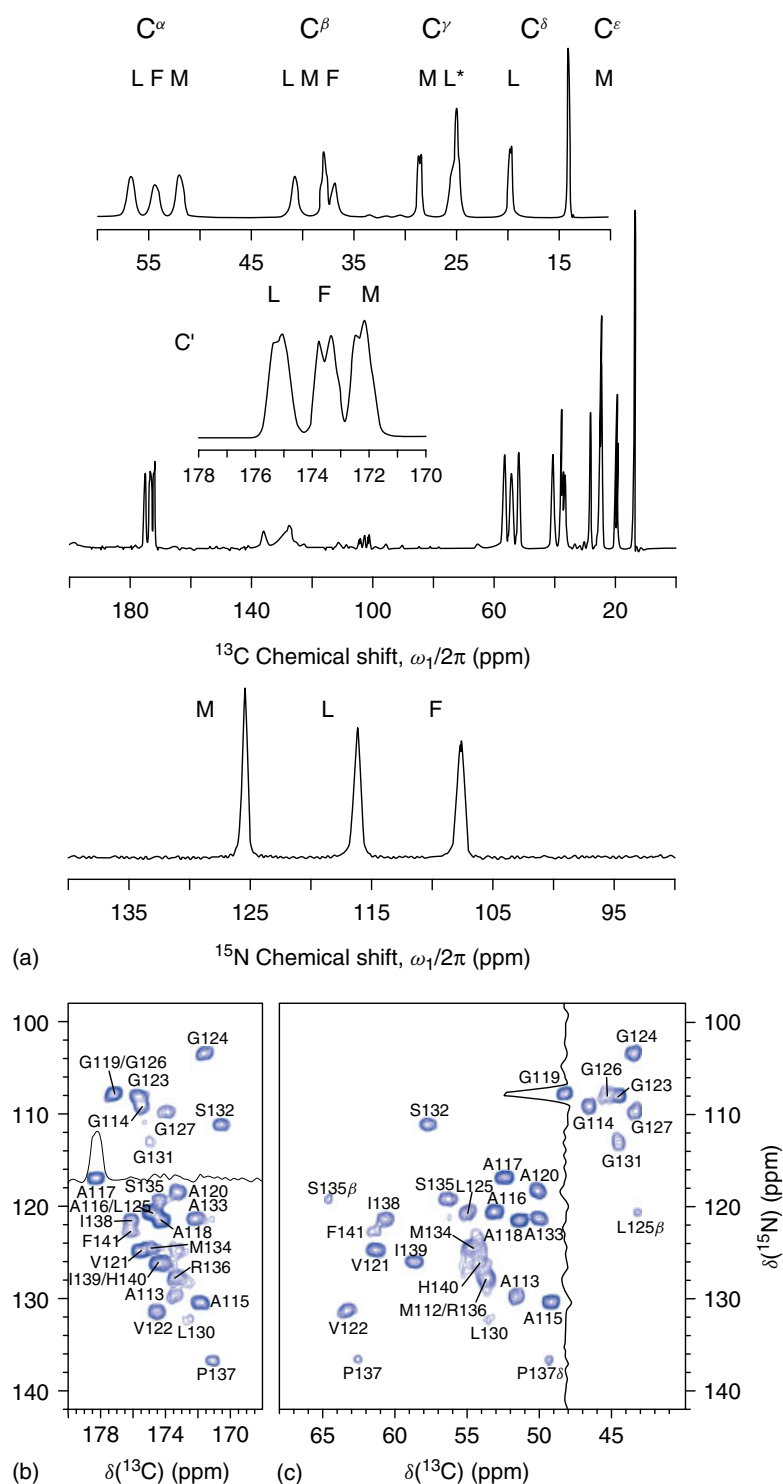


**Figure 1** (a) 1-D  $^{13}\text{C}$  and  $^{15}\text{N}$  CP-MAS spectra of formyl-U- $^{13}\text{C}$ , $^{15}\text{N}$ -Met-Leu-Phe recorded at 500 MHz  $^1\text{H}$  frequency and 8.9 kHz MAS rate. (Adapted from Ref. 47. © American Chemical Society, 2000) (b) 2-D  $^{15}\text{N}$ - $^{13}\text{C}'$  and (c)  $^{15}\text{N}$ - $^{13}\text{C}\alpha$  spectra of U- $^{13}\text{C}$ , $^{15}\text{N}$ -huPrP23-144 amyloid fibrils recorded at 500 MHz  $^1\text{H}$  frequency and 11.1 kHz MAS rate. Note that only residues comprising the relatively rigid core region of the amyloid fibrils are detected in these spectra. (Reproduced from Ref. 49. © The National Academy of Sciences of the USA, 2008.)

hand, quantitative measurements of structurally interesting, weak dipolar interactions (i.e., dipolar coupling constant  $< \approx 100$  Hz; internuclear distance  $> \approx 3$  Å) within tightly coupled spin-1/2 clusters are generally less straightforward because of the potential interference from multiple direct

and indirect spin-spin couplings, which contain little useful structural information themselves, yet are oftentimes comparable to or larger than the weak dipolar couplings of interest – in addition to the one-bond dipolar couplings listed in Table 1, these interactions include two-bond  $^{13}\text{C}$ - $^{13}\text{C}$

**Table 1** Typical magnitudes of selected one-bond dipolar couplings in peptides and proteins

Nucleus $I$	Nucleus $S$	$I$ - $S$ distance, $r_{IS}$ (Å)	$I$ - $S$ Dipolar coupling, $b_{IS}/2\pi$ (Hz)
$^1\text{H}$	$^{13}\text{C}$	1.12	21 500
$^1\text{H}$	$^{15}\text{N}$	1.04	10 825
$^{13}\text{C}$	$^{13}\text{C}$	1.52	2165
$^{13}\text{C}'$	$^{15}\text{N}$	1.33	1300
$^{13}\text{C}\alpha$	$^{15}\text{N}$	1.45	1005

and  $^{13}\text{C}$ - $^{15}\text{N}$  dipolar couplings of  $\sim 500$  Hz and  $\sim 200$  Hz, respectively, as well as one-bond  $^{13}\text{C}$ - $^{13}\text{C}$  J-couplings ( $\sim 30$ – $60$  Hz).

In this article, we focus on heteronuclear dipolar recoupling and discuss several recent SSNMR methods, which alleviate some of the major problems associated with the presence of strong dipolar and J-couplings in U- $^{13}\text{C}$ ,  $^{15}\text{N}$  enriched molecules and enable the accurate and precise measurements of multiple weak  $^{13}\text{C}$ - $^{15}\text{N}$  dipolar couplings. These methods, which include frequency-selective REDOR<sup>75,76</sup> and several 3-D transferred echo double resonance (TEDOR) variants,<sup>77-79</sup> are based on the well-known and closely related REDOR<sup>19,20</sup> and TEDOR<sup>80</sup> heteronuclear recoupling schemes, specifically selected for this purpose because they are particularly robust with respect to various experimental imperfections including finite pulse durations, resonance offsets, and RF inhomogeneity.<sup>81-87</sup> Applications of these techniques to U- $^{13}\text{C}$ ,  $^{15}\text{N}$ -enriched biological solids, ranging from small peptides and globular proteins in the microcrystalline phase to amyloid aggregates and membrane-associated proteins, are also highlighted.

## 2 MAS HAMILTONIAN

The Hamiltonian describing a system of coupled spin-1/2 nuclei placed in a strong static magnetic field and subjected to MAS and time-dependent RF fields can be written as<sup>14,16</sup>

$$\hat{H}(t) = \hat{H}_D(t) + \hat{H}_J + \hat{H}_{CS}(t) + \hat{H}_{RF}(t) \quad (1)$$

where the  $\hat{H}_D(t)$ ,  $\hat{H}_J$ ,  $\hat{H}_{CS}(t)$ , and  $\hat{H}_{RF}(t)$  terms represent direct dipolar (through-space) spin-spin couplings, indirect (through-bond) spin-spin couplings, chemical shift interactions, and applied RF fields, respectively. The individual Hamiltonian terms for a homonuclear spin system are given by

$$\hat{H}_D(t) = \sum_{i<j} \omega_{ij}^D(t) [3\hat{I}_{iz}\hat{I}_{jz} - \hat{\mathbf{I}}_i \cdot \hat{\mathbf{I}}_j] \quad (2)$$

$$\hat{H}_J = \sum_{i<j} \omega_{ij}^J \hat{\mathbf{I}}_i \cdot \hat{\mathbf{I}}_j \quad (3)$$

$$\hat{H}_{CS}(t) = \sum_i \omega_i^{CS}(t) \hat{I}_{iz} \quad (4)$$

$$\hat{H}_{RF}(t) = \sum_i |\omega_i^{RF}(t)| [\hat{I}_{ix} \cos \phi_i(t) + \hat{I}_{iy} \sin \phi_i(t)] \quad (5)$$

For heteronuclear spin pairs (and homonuclear spins, for which the absolute chemical shift difference greatly exceeds the magnitude of the spin-spin interaction, i.e.,  $|\omega_i^{CS}(t) -$

$\omega_j^{CS}(t)| \gg |\omega_{ij}^D(t)|, |\omega_{ij}^J|$ ), the dipolar and J-coupling terms simplify to

$$\hat{H}_D(t) = \sum_{i<j} \omega_{ij}^D(t) 2\hat{I}_{iz}\hat{I}_{jz} \quad (6)$$

$$\hat{H}_J = \sum_{i<j} \omega_{ij}^J \hat{I}_{iz}\hat{I}_{jz} \quad (7)$$

In equations (2–7), indices  $i$  and  $j$  refer to different nuclear spins,  $\hat{I}_x$ ,  $\hat{I}_y$ , and  $\hat{I}_z$  are the spin angular momentum operators,  $\omega_{ij}^J = 2\pi J_{ij}$  where  $J_{ij}$  is the isotropic J-coupling constant in Hz (anisotropic J-coupling terms are assumed to be negligible), and  $\omega_i^{RF}(t) = -\gamma_i B_i^{RF}(t)$  and are the RF-field angular nutation frequency (determined by the nuclear gyromagnetic ratio,  $\gamma_i$ , and RF-field amplitude,  $B_i^{RF}(t)$ ) and phase  $\phi_i(t)$ , respectively. The time-dependent coefficients  $\omega_i^{CS}(t)$  and  $\omega_{ij}^D(t)$  can be conveniently expressed as Fourier series:

$$\omega_i^{CS}(t) = \sum_{m=-2}^2 \omega_{CS_i}^{(m)} \exp(im\omega_r t) \quad (8)$$

$$\omega_{ij}^D(t) = \sum_{m=-2}^2 \omega_{D_{ij}}^{(m)} \exp(im\omega_r t) \quad (9)$$

with

$$\omega_\lambda^{(m)} = \omega_{\text{iso}}^\lambda \delta_{m,0} + \delta^\lambda \left\{ D_{0,-m}^{(2)}(\Omega_{\text{PR}}^\lambda) - \frac{\eta^\lambda}{\sqrt{6}} [D_{-2,-m}^{(2)}(\Omega_{\text{PR}}^\lambda) + D_{2,-m}^{(2)}(\Omega_{\text{PR}}^\lambda)] \right\} d_{-m,0}^{(2)}(\beta_{\text{RL}}) \quad (10)$$

where  $\lambda = \text{CS}_i$  or  $\text{D}_{ij}$ ,  $\omega_r$  is the rotor frequency in angular units,  $\delta_{m,0}$  is the Kronecker delta, and  $\omega_{\text{iso}}^\lambda$ ,  $\delta^\lambda$ , and  $\eta^\lambda$  are the isotropic value, anisotropy, and asymmetry parameter of interaction  $\lambda$ . The Wigner rotation matrices,  $D_{m',m}^{(l)}(\Omega_{\text{AB}}^\lambda)$ , describe the coordinate transformation between axis systems A and B, according to a set of three Euler angles  $\Omega_{\text{AB}}^\lambda = \{\alpha_{\text{AB}}^\lambda, \beta_{\text{AB}}^\lambda, \gamma_{\text{AB}}^\lambda\}$ <sup>88,89</sup>:

$$D_{m',m}^{(l)}(\Omega_{\text{AB}}^\lambda) = \exp(-im'\alpha_{\text{AB}}^\lambda) d_{m',m}^{(l)}(\beta_{\text{AB}}^\lambda) \exp(-im\gamma_{\text{AB}}^\lambda) \quad (11)$$

where  $d_{m',m}^{(l)}(\beta_{\text{AB}}^\lambda)$  is the reduced Wigner matrix. The coordinate systems most relevant to the description of MAS NMR experiments in polycrystalline solids are denoted as P

(principal axis frame), C (crystallite-fixed frame), R (rotor-fixed frame), and L (laboratory frame). Note that, for simplicity, equation (10) assumes that the principal axis frame coincides with the crystallite-fixed frame.

For the dipolar coupling between spins  $i$  and  $j$  we have

$$\omega_{\text{iso}}^{\text{D}_{ij}} = \eta^{\text{D}_{ij}} = 0 \quad (12)$$

$$\delta^{\text{D}_{ij}} = b_{ij} = -\left(\frac{\mu_0}{4\pi}\right) \frac{\gamma_i \gamma_j \hbar}{r_{ij}^3} \quad (13)$$

where  $b_{ij}$  is the dipolar coupling constant in angular frequency units and  $r_{ij}$  is the internuclear distance. Thus, for macroscopic sample rotation exactly at the magic angle,  $\beta_{\text{RL}} = \tan^{-1} \sqrt{2}$ , the Fourier coefficients in equations (8–10) are given by

$$\omega_{\text{D}_{ij}}^{(0)} = b_{ij} \frac{(3 \cos^2 \beta_{\text{PR}}^{ij} - 1)}{2} \frac{(3 \cos^2 \beta_{\text{RL}} - 1)}{2} = 0 \quad (14)$$

$$\omega_{\text{D}_{ij}}^{(\pm 1)} = -\frac{1}{2\sqrt{2}} b_{ij} \sin(2\beta_{\text{PR}}^{ij}) \exp(\pm i\gamma_{\text{PR}}^{ij}) \quad (15)$$

$$\omega_{\text{D}_{ij}}^{(\pm 2)} = \frac{1}{4} b_{ij} \sin^2 \beta_{\text{PR}}^{ij} \exp(\pm i2\gamma_{\text{PR}}^{ij}) \quad (16)$$

Analogous expressions can also be obtained for the chemical shift interaction,<sup>3,14,17</sup> where  $\omega_{\text{iso}}^{\text{CS}_i}$ ,  $\delta^{\text{CS}_i}$ , and  $\eta^{\text{CS}_i}$  are, in general, nonzero. Altogether, equations (8–16) demonstrate the well-known result that MAS effectively averages anisotropic nuclear spin interactions described by second-rank tensors<sup>1–3</sup> – the time-independent Fourier coefficients,  $\omega_{\lambda}^{(0)}$ , vanish when  $\beta_{\text{RL}}$  is the magic angle, and the  $\omega_{\lambda}^{(\pm 1)}$  and  $\omega_{\lambda}^{(\pm 2)}$  coefficients oscillating at  $\omega_r$  and  $2\omega_r$  are averaged to zero with the period of one and one-half rotor cycle, respectively.

### 3 HETERONUCLEAR DIPOLAR RECOUPLING IN SPIN PAIRS

In this section, we briefly review several methods designed to reintroduce heteronuclear dipolar interactions under MAS in isolated spin pairs, with the main focus on rotary resonance recoupling ( $\text{R}^3$ )<sup>90,91</sup> and REDOR.<sup>19,20</sup> These initial recoupling schemes have not only been utilized for a variety of diverse applications,<sup>16,22</sup> but their introduction has also motivated the development of a multitude of new dipolar recoupling methodologies – indeed, as noted above, the recoupling techniques designed to measure weak  $^{13}\text{C}$ – $^{15}\text{N}$  dipolar couplings in  $\text{U}$ - $^{13}\text{C}$ ,  $^{15}\text{N}$  labeled systems, which are discussed in the following section, are all derived from the REDOR recoupling scheme. To gain basic insight into how the application of RF pulse sequences can interfere with MAS to reintroduce heteronuclear dipolar couplings, in the following, we consider a simple system of two coupled nuclear spins of different types, denoted by  $\text{I}_1$  and  $\text{I}_2$ , in the absence of chemical shift and J-coupling interactions.

#### 3.1 Rotary Resonance Recoupling

$\text{R}^3$  involves the observation of the NMR signal for spin species  $\text{I}_1$ , in the presence of continuous-wave RF irradiation applied to spin species  $\text{I}_2$ , where the RF nutation frequency is set to a small integer multiple of the MAS frequency ( $\omega_2^{\text{RF}} = n\omega_r$ ).<sup>90,91</sup> The corresponding Hamiltonian, assuming that  $\omega_2^{\text{RF}}$  has phase  $x$ , is given by

$$\hat{H}(t) = \omega_{12}^{\text{D}}(t) 2\hat{I}_{1z}\hat{I}_{2z} + n\omega_r \hat{I}_{2x} \quad (17)$$

The combined effects of MAS and rotor-synchronized RF pulse sequences on nuclear spin dynamics can be conveniently analyzed within the framework of the average Hamiltonian theory (AHT)<sup>92,93</sup> (see *Average Hamiltonian Theory*) – this involves the transformation of  $\hat{H}(t)$  into an interaction frame where the  $\hat{H}_{\text{RF}}(t)$  term vanishes, followed by calculation of the effective (or average) Hamiltonian describing the internal nuclear spin interactions (i.e., chemical shifts, dipolar, and J-couplings). For the  $\text{R}^3$  experiment, the interaction frame dipolar Hamiltonian is given by

$$\begin{aligned} \tilde{\hat{H}}_{\text{D}}(t) &= e^{in\omega_r t} \hat{I}_{2x} \hat{H}_{\text{D}}(t) e^{-in\omega_r t} \hat{I}_{2x} \\ &= \sum_{m=-2}^2 \left\{ \omega_{\text{D}_{12}}^{(m)} [e^{i(m+n)\omega_r t} + e^{i(m-n)\omega_r t}] \hat{I}_{1z} \hat{I}_{2z} \right. \\ &\quad \left. - i\omega_{\text{D}_{12}}^{(m)} [e^{i(m+n)\omega_r t} - e^{i(m-n)\omega_r t}] \hat{I}_{1z} \hat{I}_{2y} \right\} \quad (18) \end{aligned}$$

and the lowest-order effective Hamiltonian,  $\overline{\hat{H}}_{\text{D}}^{(0)}$ , is obtained as the average of the interaction frame Hamiltonian over the pulse sequence cycle time (one rotor period,  $\tau_r$ , in this case):

$$\overline{\hat{H}}_{\text{D}}^{(0)} = \frac{1}{\tau_r} \int_0^{\tau_r} dt \tilde{\hat{H}}_{\text{D}}(t) \quad (19)$$

Since all integrals of the form  $\int_0^{\tau_r} dt \exp[i(m \pm n)\omega_r t]$  that appear in equations (18) and (19) vanish unless a rotary resonance condition  $m \pm n = 0$  is satisfied, the lowest-order average dipolar Hamiltonian is given by

$$\overline{\hat{H}}_{\text{D}}^{(0)} = (\omega_{\text{D}_{12}}^{(-n)} + \omega_{\text{D}_{12}}^{(n)}) \hat{I}_{1z} \hat{I}_{2z} - i(\omega_{\text{D}_{12}}^{(-n)} - \omega_{\text{D}_{12}}^{(n)}) \hat{I}_{1z} \hat{I}_{2y} \quad (20)$$

This result indicates that dipolar coupling terms corresponding to coefficients  $\omega^{(\pm 1)}$  and  $\omega^{(\pm 2)}$  (cf. equations (15) and (16)) are reintroduced under MAS when the RF nutation frequency equals  $\omega_r$  and  $2\omega_r$ , respectively – otherwise  $\overline{\hat{H}}_{\text{D}}^{(0)} = 0$  and heteronuclear decoupling is predicted at this level of AHT treatment. For example, for  $n = \pm 1$   $\text{R}^3$  we have

$$\overline{\hat{H}}_{\text{D}}^{(0)} = \tilde{\omega}_{12}^{\text{D}} (\cos \gamma_{\text{PR}}^{12} 2\hat{I}_{1z}\hat{I}_{2z} - \sin \gamma_{\text{PR}}^{12} 2\hat{I}_{1z}\hat{I}_{2y}) \quad (21)$$

where the orientation-dependent effective dipolar coupling,  $\tilde{\omega}_{12}^{\text{D}}$ , is given by

$$\tilde{\omega}_{12}^{\text{D}} = -\frac{1}{2\sqrt{2}} b_{12} \sin(2\beta_{\text{PR}}^{12}) \quad (22)$$

With the initial density operator  $\hat{\rho}(0) = \hat{I}_{1x}$ , the evolution under the average Hamiltonian in equation (21) yields an observable  $I_1$ -spin signal of the following form:

$$S(\tau_{\text{mix}}) = \langle \hat{I}_{1x} \rangle (\tau_{\text{mix}}) = \langle \cos(\tilde{\omega}_{12}^D \tau_{\text{mix}}) \rangle \quad (23)$$

where  $\langle \dots \rangle$  indicates the powder average, and, consequently, the magnitude of the  $I_1$ - $I_2$  dipolar coupling constant,  $b_{12}$ , can be extracted in a straightforward manner by inspecting the  $I_1$ -spin evolution in the time or frequency domain (Figure 2). Note that the magnitude of the dipolar interaction recoupled by  $R^3$  is independent of the Euler angle  $\gamma_{\text{PR}}^{12}$  – this property of the recoupling sequence, commonly referred to as  $\gamma$ -encoding,<sup>94</sup> leads to particularly pronounced dipolar oscillations as seen in Figure 2(a).

The simple analysis above clearly demonstrates the emergence of dipolar recoupling conditions resulting from the interference between MAS and applied RF fields, and also provides a reasonable approximation to the  $I_1$ -spin dynamics in cases where the  $I_1$ - $I_2$  dipolar coupling is the dominant interaction. However, typically, the spin dynamics during  $R^3$  are far more complicated owing to their strong concurrent dependence on the chemical shift tensor parameters of the  $I_2$ -spin. This stems

from the fact that  $R^3$  also reintroduces  $I_2$ -spin CSA terms (described by an effective Hamiltonian analogous to  $\overline{\hat{H}}_D^{(0)}$ , but with  $\hat{I}_{1z}$  omitted and  $\tilde{\omega}_{12}^D$  replaced by  $\tilde{\omega}_2^{\text{CS}}$ ), which, in general, do not commute with the  $I_1$ - $I_2$  dipolar coupling and lead to significant distortions of the  $n = \pm 1$  and  $\pm 2$   $R^3$  dipolar trajectories as well as the appearance of additional, albeit weaker, higher order ( $|n| > 2$ ) rotary resonances.<sup>14,16,91</sup> Another potential disadvantage associated with  $R^3$  is its sensitivity to RF inhomogeneity.<sup>90,91</sup>

While  $R^3$  itself may oftentimes not be the method of choice for quantitative measurements of heteronuclear dipolar couplings, several closely related schemes have been proposed to alleviate the problems associated with the dependence of  $R^3$  dipolar dephasing trajectories on the CSA parameters of the irradiated spin as well as RF inhomogeneity.<sup>63,96,97</sup> For example the SPI- $R^3$  sequence,<sup>63</sup> which involves the application of a rotary resonant RF field to the  $I_2$ -spin  $\omega_2^{\text{RF}} = n\omega_r$  that is also continuously phase inverted during successive rotor cycles, is relatively insensitive to both  $I_2$  CSA and RF inhomogeneity. Such rotor-synchronized  $\pm x$  phase alternation of  $\omega_2^{\text{RF}}$  has no effect on the  $\hat{I}_{1z}\hat{I}_{2z}$  term in equation (21) but repeatedly changes the sign of the  $\hat{I}_{1z}\hat{I}_{2y}$  term, meaning that after every two rotor periods the latter term is averaged to zero. The lowest order average dipolar Hamiltonian for  $n = \pm 1$  SPI- $R^3$  is thus given by

$$\overline{\hat{H}}_D^{(0)} = \tilde{\omega}_{12}^D 2\hat{I}_{1z}\hat{I}_{2z} \quad (24)$$

with

$$\tilde{\omega}_{12}^D = -\frac{1}{2\sqrt{2}}b_{12}\sin(2\beta_{\text{PR}}^{12})\cos\gamma_{\text{PR}}^{12} \quad (25)$$

More importantly, since the effective chemical shift Hamiltonian for SPI- $R^3$ ,  $\overline{\hat{H}}_{\text{CS}}^{(0)} \propto \hat{I}_{2z}$ , now commutes with  $\overline{\hat{H}}_D^{(0)}$ , it has no influence on  $I_1$ -spin dynamics to lowest order – i.e., the  $I_1$  dipolar dephasing trajectory,  $S(\tau_{\text{mix}}) = \langle \cos(\tilde{\omega}_{12}^D \tau_{\text{mix}}) \rangle$ , reports primarily on the magnitude of  $b_{12}$ . We note here that although the attenuation of the effects of  $I_2$ -spin CSA and RF inhomogeneity by SPI- $R^3$  is associated with the fact that the pulse sequence is no longer  $\gamma$ -encoded ( $\tilde{\omega}_{12}^D$  in equation (25) depends on both  $\beta_{\text{PR}}^{12}$  and  $\gamma_{\text{PR}}^{12}$ ), which leads to somewhat less pronounced dipolar oscillations, this does not have a significant negative impact on the accurate determination of heteronuclear dipolar couplings.

### 3.2 Rotational Echo Double Resonance

While  $R^3$  and related pulse schemes discussed in the previous section are all windowless, heteronuclear dipolar recoupling can also be achieved by applying sequences of discrete, rotor-synchronized  $180^\circ$  pulses to one or both spin species. This idea forms the basis for the REDOR technique developed by Gullion and Schaefer.<sup>19,20</sup> A typical implementation of REDOR, with all  $180^\circ$  recoupling pulses – two per rotor period – applied to the nonobserved  $I_2$  spin species (usually  $^{15}\text{N}$  in the context of  $^{13}\text{C}$ - $^{15}\text{N}$  spin pair labeled samples) is shown in Figure 3. Note that the  $I_1$  signal during REDOR is generally observed as a spin-echo – therefore, for the pulse sequence in Figure 3 the entire group of

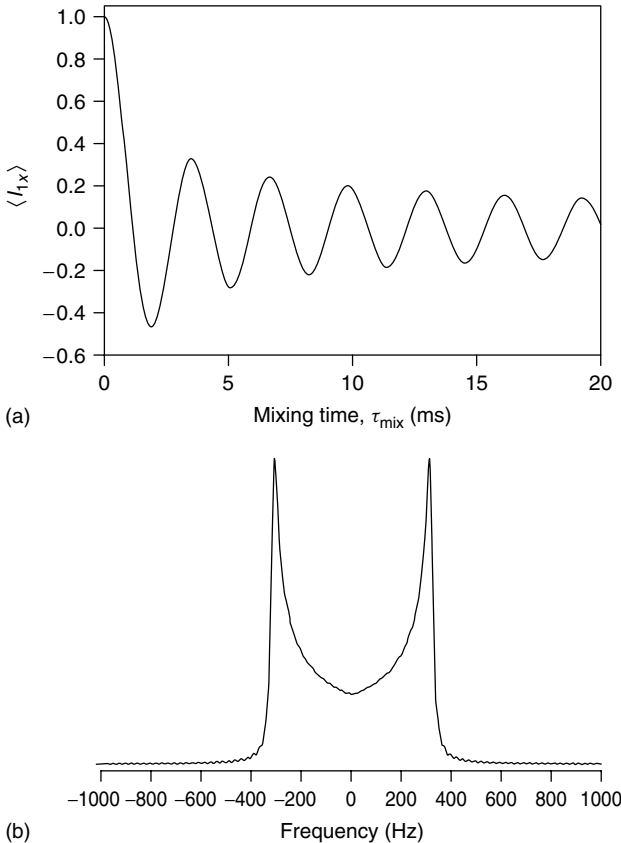


**Figure 2** Simulated  $I_1$ -spin dipolar dephasing trajectory (a) and spectrum (b) corresponding to a  $n = \pm 1$  rotary resonance recoupling experiment. The simulation was performed by the stepwise numerical propagation of the density operator for a heteronuclear  $I_1$ - $I_2$  ( $^{13}\text{C}$ - $^{15}\text{N}$ ) spin pair with a dipolar coupling constant,  $b_{12}/2\pi = 900$  Hz, in the absence of chemical shifts and J-coupling, as implemented within the SIMPSON program.<sup>95</sup> The MAS rate and  $I_2$ -spin RF nutation frequency were set to 25 kHz

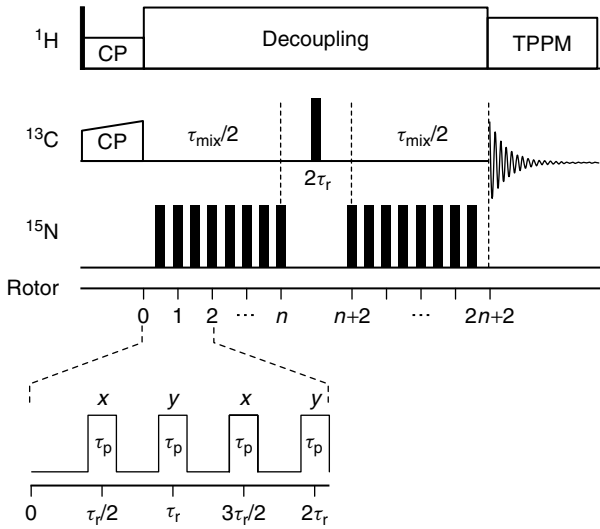


**Figure 3** A typical implementation of the REDOR pulse sequence.<sup>19,20</sup> The particular implementation shown is especially relevant to studies of U-<sup>13</sup>C, <sup>15</sup>N labeled molecules. Narrow and wide black rectangles correspond to 90° and 180° pulses. During the REDOR experiment a <sup>13</sup>C spin-echo is generated following <sup>1</sup>H–<sup>13</sup>C CP. The echo intensity is modulated during the period  $\tau_{\text{mix}}$  according to the magnitude of the <sup>13</sup>C–<sup>15</sup>N dipolar coupling, reintroduced by applying a train of rotor-synchronized 180° pulses on the <sup>15</sup>N channel as indicated in the figure. The <sup>15</sup>N pulse phases are usually set according to the *xy*-4 (*xyxy*) or *xy*-8 (*xyxy yxyx*) schemes,<sup>81</sup> which offer a high degree of compensation for pulse imperfections. Note that REDOR experiments generally involve the acquisition of two separate spin-echo trajectories: the dipolar dephased trajectory ( $S$ ) using the pulse scheme shown in the figure, and a reference trajectory ( $S_0$ ) that accounts for the transverse relaxation of <sup>13</sup>C coherences not related to <sup>13</sup>C–<sup>15</sup>N dipolar dephasing. The  $S_0$  trajectory is typically recorded in the absence of <sup>15</sup>N 180° pulses, although implementations that involve the application of an additional <sup>15</sup>N refocusing 180° pulse<sup>85</sup> or the time-shifting of a part of the <sup>15</sup>N 180°-pulse train can also be used<sup>76,86</sup> (cf. Figure 5). The resulting REDOR trajectories are then displayed as  $S/S_0$  or  $\Delta S/S_0 = 1 - S/S_0$

<sup>15</sup>N 180° pulses following the 180° <sup>13</sup>C pulse is time-shifted by  $\tau_r/2$  relative to the pulses preceding the <sup>13</sup>C 180° to prevent the refocusing of the recoupled <sup>13</sup>C–<sup>15</sup>N dipolar interaction.

Assuming ideal  $\delta$ -function 180° pulses for the time being, the interaction frame dipolar Hamiltonian for the REDOR scheme is given by

$$\tilde{H}_D(t) = f(t)\omega_{12}^D(t)2\hat{I}_{1z}\hat{I}_{2z} \quad (26)$$

where  $\omega_{12}^D(t)$  is defined in equation (9), and the function  $f(t)$  toggles between the values of  $\pm 1$  during subsequent delays between 180° pulses. A straightforward calculation of the lowest order average dipolar Hamiltonian using equation (19), assuming the 180° pulses are applied on the  $I_2$  channel at  $\tau_r/2$  intervals as shown in Figure 3, yields

$$\overline{\tilde{H}_D}^{(0)} = \tilde{\omega}_{12}^D 2\hat{I}_{1z}\hat{I}_{2z} \quad (27)$$

with

$$\tilde{\omega}_{12}^D = -\frac{\sqrt{2}}{\pi}b_{12}\sin(2\beta_{\text{PR}}^{12})\sin\gamma_{\text{PR}}^{12} \quad (28)$$

Note that the form of the effective dipolar Hamiltonian for REDOR closely resembles that for  $n = \pm 1$  SPI-R<sup>3</sup> (see equations (24) and (25)), with the main difference being the magnitude of the dipolar scaling factor ( $\frac{\sqrt{2}}{\pi} \approx 0.45$  for REDOR vs.  $\frac{1}{2\sqrt{2}} \approx 0.35$  for SPI-R<sup>3</sup>; a higher scaling factor is generally advantageous). This indicates that, in analogy to SPI-R<sup>3</sup>, the REDOR scheme shown in Figure 3 is also relatively insensitive to the recoupled  $I_2$ -spin CSA.

In practice, REDOR experiments are susceptible to various experimental imperfections including resonance offsets and RF inhomogeneity – particularly challenging are the measurements of weak dipolar couplings, which require the application of tens to hundreds of rotor-synchronized 180° pulses. This major problem was addressed shortly following the introduction of REDOR via the design of *xy*-type 180° pulse phasing schemes (e.g., *xy*-4: *xyxy*, *xy*-8: *xyxy yxyx*, etc.; see Figure 3), which offer a very high degree of compensation for such experimental imperfections.<sup>81,82</sup> More recently, additional improvements involving the use of composite 180° pulses have also been proposed.<sup>87</sup> Altogether, these developments have resulted in REDOR being a particularly robust heteronuclear dipolar recoupling pulse scheme, which has been successfully applied for the measurements of weak dipolar couplings in a number of complex biological systems.<sup>16,22</sup>

An additional potential concern related to the use of REDOR-type methods, which is not a factor for windowless recoupling schemes, is related to the effect of finite 180° pulse lengths on the recoupling performance (see *Accuracy Limitations on Internuclear Distances Measured by REDOR*). This is a rather important issue, given that many modern SSNMR experiments routinely take advantage of high MAS rates in the  $\sim 10$ – $40$  kHz regime to achieve optimal spectral resolution and sensitivity. For example, for the REDOR scheme in Figure 3 implemented with a typical  $I_2$ -spin RF nutation frequency,  $\omega_2^{\text{RF}}/2\pi = 50$  kHz, but at an MAS rate of 30 kHz instead of the usual 5–6 kHz,  $\sim 60\%$  of the rotor period would be occupied by RF irradiation. The effects of finite pulses on the spin dynamics during REDOR have been analyzed using Floquet theory<sup>83</sup> as well as AHT and numerical simulations.<sup>84</sup> The overall conclusion of these studies is that finite pulse effects do not negatively impact the performance of REDOR recoupling provided that *xy*-4 type 180° pulse phasing schemes are employed, which is virtually always the case. We summarize below the AHT treatment for REDOR *xy*-4 and related sequences, which yields analytical expressions describing the spin dynamics in the presence of finite pulse effects<sup>84</sup> – for purpose of comparison, we also discuss a hypothetical implementation of REDOR where all pulse phases are *x*. Finally, an experimental demonstration of the finite pulse effects for REDOR *xy*-4 type schemes is provided.

In general, the interaction frame Hamiltonian for the REDOR sequence in Figure 3 in the presence of finite 180° pulses of arbitrary phase can be written:

$$\tilde{H}_D(t) = \omega_{12}^D(t)[f(t)2\hat{I}_{1z}\hat{I}_{2z} + g(t)2\hat{I}_{1z}\hat{I}_{2x} + h(t)2\hat{I}_{1z}\hat{I}_{2y}] \quad (29)$$

In analogy to equation (26), the function  $f(t)$  toggles, albeit in a continuous manner, between  $\pm 1$  during subsequent delays between pulses regardless of the details of the pulse phase

cycling scheme. The functions  $g(t)$  and  $h(t)$  are a direct consequence of the finite pulses – they can only be nonzero during the pulses and their values depend on the details of the phase cycling scheme. For example, for REDOR  $xy$ -4 both  $g(t)$  and  $h(t)$  take on nonzero values, while  $g(t)$  is always zero if all recoupling pulses have phase  $x$ . Although the presence of terms proportional to operators  $\hat{I}_{2x}$  and/or  $\hat{I}_{2y}$  in the effective dipolar Hamiltonian would generally be expected to have a negative impact on the performance of REDOR recoupling – these terms would not only significantly perturb the dipolar dephasing trajectories predicted for  $\delta$ -function pulses but their appearance would also indicate the concurrent recoupling of noncommuting  $I_2$  CSA terms – it turns out that for REDOR  $xy$ -4 and extensions thereof these transverse  $I_2$ -spin terms are averaged to zero with a cycle time of two rotor periods. The resulting lowest order average dipolar Hamiltonian for REDOR  $xy$ -4 with finite pulses is

$$\overline{\hat{H}}_D^{(0)} = \tilde{\omega}_{12}^D 2\hat{I}_{1z}\hat{I}_{2z} \quad (30)$$

where

$$\tilde{\omega}_{12}^D = -\frac{\sqrt{2}}{\pi}\kappa b_{12} \sin(2\beta_{\text{PR}}^{12}) \sin \gamma_{\text{PR}}^{12} \quad (31)$$

Note that the effective dipolar Hamiltonian for finite pulse REDOR  $xy$ -4 is nearly identical to the Hamiltonian for  $\delta$ -pulse REDOR (cf. equations (27) and (28)). The only difference is the factor  $\kappa$  in equation (31), which describes the finite pulse effects and is given by

$$\kappa = \frac{\cos(\varphi\pi/2)}{1 - \varphi^2} \quad (32)$$

where  $\varphi$  is the fraction of the rotor period occupied by the pulses:

$$\varphi = \frac{2\tau_p}{\tau_r} \quad (33)$$

For  $\delta$ -pulse REDOR we have  $\varphi = 0$ , which gives  $\kappa = 1$ , and, as expected, equation (31) reduces to equation (28). At the other extreme, in the case of windowless RF irradiation (i.e.,  $\varphi = 1$ ) we obtain  $\lim_{\varphi \rightarrow 1} \kappa = \pi/4$ . This yields the effective dipolar coupling of

$$\tilde{\omega}_{12}^D = -\frac{1}{2\sqrt{2}}b_{12} \sin(2\beta_{\text{PR}}^{12}) \sin \gamma_{\text{PR}}^{12} \quad (34)$$

which is analogous to the expression obtained for SPI-R<sup>3</sup> (cf. equation (25)). For a typical intermediate case involving rapid MAS (e.g.,  $\omega_2^{\text{RF}}/2\pi = 50$  kHz and  $\omega_r/2\pi = 30$  kHz), we have  $\varphi \approx 0.61$  and  $\kappa \approx 0.92$  – i.e., AHT predicts that the dipolar coupling is reduced by only  $\sim 8\%$  relative to that expected in the  $\delta$ -pulse limit. Given that this additional scaling of the dipolar coupling can be readily accounted for in simulations by simply specifying the value of  $\varphi$ , the finite pulse effects for REDOR  $xy$ -4 and its extensions are relatively harmless.

For comparison, we briefly consider below a finite pulse version of the REDOR scheme where all  $180^\circ$  pulses on the  $I_2$  channel have phase  $x$ . In this case, transverse  $I_2$ -spin terms appear in the average dipolar Hamiltonian,

which leads to significant perturbations of the REDOR dipolar dephasing trajectories as well as increased dependence of these trajectories on  $I_2$  CSA parameters. The lowest order average dipolar Hamiltonian in this case is given by

$$\overline{\hat{H}}_D^{(0)} = -\frac{\sqrt{2}}{\pi}\kappa b_{12} \sin(2\beta_{\text{PR}}^{12}) \times [\sin \gamma_{\text{PR}}^{12} 2\hat{I}_{1z}\hat{I}_{2z} + \varphi \cos \gamma_{\text{PR}}^{12} 2\hat{I}_{1z}\hat{I}_{2y}] \quad (35)$$

which leads to the observable signal of the form

$$S(\tau_{\text{mix}}) = \langle \cos(\sqrt{\Omega^2 + \Phi^2}\tau_{\text{mix}}) \rangle \quad (36)$$

with

$$\Omega = -\frac{\sqrt{2}}{\pi}\kappa b_{12} \sin(2\beta_{\text{PR}}^{12}) \sin \gamma_{\text{PR}}^{12} \quad (37)$$

$$\Phi = -\frac{\sqrt{2}}{\pi}\varphi\kappa b_{12} \sin(2\beta_{\text{PR}}^{12}) \cos \gamma_{\text{PR}}^{12} \quad (38)$$

Note that in the case of windowless  $x$ -phase RF irradiation ( $\varphi = 1$ ,  $\kappa = \pi/4$ ) the observable signal in equations (36–38) reduces to the  $\gamma_{\text{PR}}^{12}$ -independent expression obtained for  $n = \pm 1$  R<sup>3</sup> (cf. equations (22) and (23)).

In Figure 4, we provide an experimental verification of the finite pulse effects for REDOR  $xy$ -4 type sequences.<sup>84</sup> Figure 4(a) shows representative experimental and simulated REDOR  $S/S_0$  trajectories for 2-<sup>13</sup>C,<sup>15</sup>N-glycine, recorded under experimental conditions where 20% ( $\varphi = 0.2$ ;  $\omega_2^{\text{RF}}/2\pi = 50$  kHz and  $\omega_r/2\pi = 10$  kHz) and 61% ( $\varphi = 0.61$ ;  $\omega_2^{\text{RF}}/2\pi = 25$  kHz and  $\omega_r/2\pi \approx 15.1$  kHz) of the rotor period is occupied by RF pulses. These trajectories clearly demonstrate the minor scaling of the dipolar oscillation frequency predicted above by AHT. Figure 4(b) shows the quantitative analysis of these data, where we plot the effective dipolar coupling extracted from several REDOR dephasing trajectories recorded for  $\varphi$  values in the range 0.1 to 0.61. The experimental dipolar couplings are generally found to be in good agreement with the corresponding values predicted by the AHT analysis.

### 3.3 Symmetry-Based Pulse Sequences

Recently, starting with a scheme designed to achieve broadband  $\gamma$ -encoded homonuclear <sup>13</sup>C–<sup>13</sup>C double-quantum dipolar recoupling,<sup>98</sup> Levitt and coworkers have introduced a family of general rotor-synchronized symmetry-based recoupling pulse sequences<sup>99–101</sup> (see *Symmetry-Based Pulse Sequences in Magic-Angle Spinning Solid-State NMR*). In the context of heteronuclear dipolar recoupling, some of these symmetry-based sequences can be viewed as extensions of the R<sup>3</sup> and REDOR schemes. The two most widely explored symmetry classes are denoted  $CN_n^\nu$  and  $RN_n^\nu$ , where  $N$ ,  $n$ , and  $\nu$  are referred to as the symmetry numbers of the pulse sequence. In the case of  $CN_n^\nu$  sequences, a total of  $N$   $C$ -elements or cycles, each corresponding to a rotation of nuclear spins by an integer multiple of  $360^\circ$ , are incorporated into  $n$  rotor periods. Concurrently, the RF phases of subsequent  $C$ -elements are

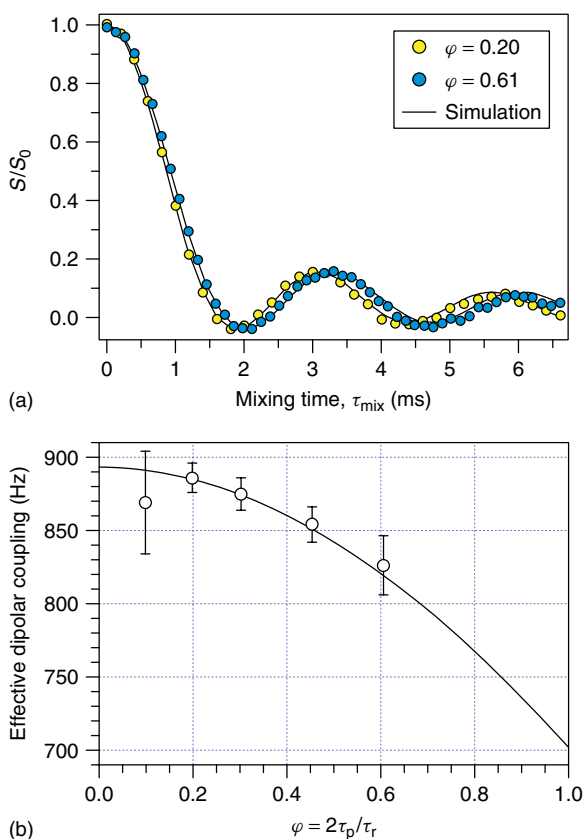


**Figure 4** Finite pulse effects in REDOR experiments. (a) Representative experimental and simulated REDOR  $S/S_0$  trajectories for  $2\text{-}^{13}\text{C},^{15}\text{N}$ -glycine. The trajectories shown were recorded under experimental conditions, where 20% ( $\varphi = 0.20$ ; yellow circles) or 61% ( $\varphi = 0.61$ ; blue circles) of the rotor cycle is occupied by the REDOR  $180^\circ$  pulses on the  $^{15}\text{N}$  channel. (b) Plot of the measured effective  $^{15}\text{N}\text{-}^{13}\text{C}\alpha$  dipolar couplings,  $b_{IS}^{\text{eff}}/2\pi$ , in  $2\text{-}^{13}\text{C},^{15}\text{N}$ -glycine as a function of the fraction of the rotor cycle occupied by REDOR pulses,  $\varphi$ . The error bars are  $\pm 2\sigma$ . The solid line corresponds to a  $b_{IS}^{\text{eff}}$  vs.  $\varphi$  curve predicted using average Hamiltonian theory,  $b_{IS}^{\text{eff}}/2\pi = (b_{IS}/2\pi) \times \cos(\varphi\pi/2)/(1 - \varphi^2)$ , where  $b_{IS}/2\pi = 894$  Hz is the dipolar coupling expected in the  $\delta$ -pulse limit. (Adapted from Ref. 84. © Elsevier Science, 2000.)

incremented with respect to each other by the angle  $2\pi\nu/N$ . The implementation of  $RN_n^v$  sequences is similar to  $CN_n^v$  sequences in that  $N$   $R$ -elements are accommodated within  $n$  rotor periods. However, each  $R$ -element induces a  $180^\circ$  rather than a  $360^\circ$  rotation of the nuclear spins, and the RF phase is alternated between the values of  $\pm\pi\nu/N$  rather than being repeatedly incremented.

While a detailed discussion of the various symmetry-based pulse schemes is beyond the scope of this article, the fundamental principle behind sequences of this type is that, by satisfying periodic symmetry relationships between the mechanical sample rotation due to MAS and RF rotations imposed by the pulse sequence, the space and spin trajectories for the different nuclear spin interactions (represented by quantum numbers  $l$  and  $m$ , and  $\lambda$  and  $\mu$ , respectively) can be synchronized to generate an average Hamiltonian that suppresses all  $\{l, m, \lambda, \mu\}$  combinations except for the desired ones. This means that it is possible to design pulse schemes, which permit highly selective recoupling of the nuclear spin

interactions of interest. For example, we have noted above that in addition to recoupling heteronuclear dipolar couplings both SPI-R<sup>3</sup> and REDOR schemes also recouple the CSA of the irradiated spins. While such CSA recoupling is unavoidable for single-channel pulse sequences designed to achieve heteronuclear dipolar recoupling, both REDOR and SPI-R<sup>3</sup> can also reintroduce homonuclear dipolar couplings between the irradiated spins, which may interfere with heteronuclear dipolar evolution in some spin systems. Certain symmetry-based pulse sequences ( $R12_3^1$ ,  $R16_4^1$ , etc.; see *Symmetry-Based Pulse Sequences in Magic-Angle Spinning Solid-State NMR*<sup>(9)</sup> for details) generate an effective dipolar Hamiltonian  $\overline{H}_D^{(0)} \propto \hat{I}_{1z}\hat{I}_{2z}$  that is analogous to that for REDOR and SPI-R<sup>3</sup>, but with concurrent suppression of homonuclear dipolar couplings. An alternative approach to suppressing homonuclear dipolar couplings in REDOR and SPI-R<sup>3</sup> experiments, based on the symmetries  $C3_3^1$  and  $C7_7^1$ , has also been proposed.<sup>102</sup>

#### 4 HETERONUCLEAR DIPOLAR RECOUPLING IN MULTISPIN SYSTEMS

While measurements of interatomic distances in heteronuclear  $^{13}\text{C}\text{-}^{15}\text{N}$  spin pairs using SSNMR methods described in the section “Heteronuclear Dipolar Recoupling Spin Pairs” are relatively routine nowadays,<sup>16,22</sup> the extension of these experiments to  $\text{U-}^{13}\text{C},^{15}\text{N}$  labeled systems has generally not been straightforward owing to the presence of multiple homonuclear and heteronuclear spin–spin couplings. This problem is particularly exacerbated for measurements of weak  $^{13}\text{C}\text{-}^{15}\text{N}$  dipolar couplings, which correspond to structurally interesting distances of greater than  $\sim 3$  Å. For example, as discussed in more detail below, if the REDOR scheme in Figure 3 were applied to a molecule containing multiple coupled  $^{13}\text{C}$  and  $^{15}\text{N}$  nuclei, the resulting  $^{13}\text{C}$  dephasing trajectories would be dominated by the strongest  $^{13}\text{C}\text{-}^{15}\text{N}$  dipolar interactions. Furthermore, the simultaneous evolution of  $^{13}\text{C}$  magnetization under the  $\sim 30\text{--}60$  Hz one-bond  $^{13}\text{C}\text{-}^{13}\text{C}$  J-couplings would lead to an additional modulation of these trajectories and generate antiphase  $^{13}\text{C}$  coherences, especially for long mixing

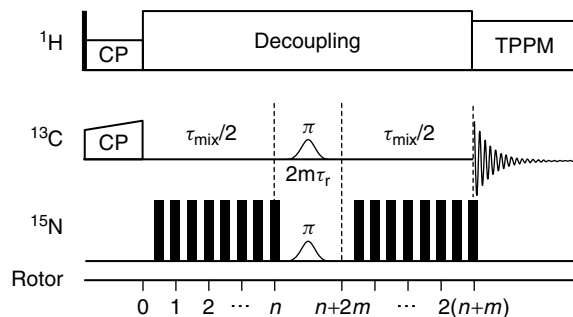


**Figure 5** Frequency-selective REDOR pulse sequence.<sup>76</sup> The recoupling of individual  $^{13}\text{C}\text{-}^{15}\text{N}$  spin pairs in  $\text{U-}^{13}\text{C},^{15}\text{N}$  labeled molecules with concurrent suppression of  $^{13}\text{C}\text{-}^{13}\text{C}$  J-couplings is achieved by using a pair of rotor-synchronized frequency-selective (e.g., Gaussian-shaped)  $180^\circ$  pulses applied simultaneously on the  $^{13}\text{C}$  and  $^{15}\text{N}$  channels as indicated in the figure. The REDOR dipolar dephasing  $S$  trajectory is recorded using the pulse scheme as shown, and the reference  $S_0$  trajectory is recorded in the absence of the selective  $^{15}\text{N}$  pulse. See the caption to Figure 3 for additional details of the REDOR pulse sequence

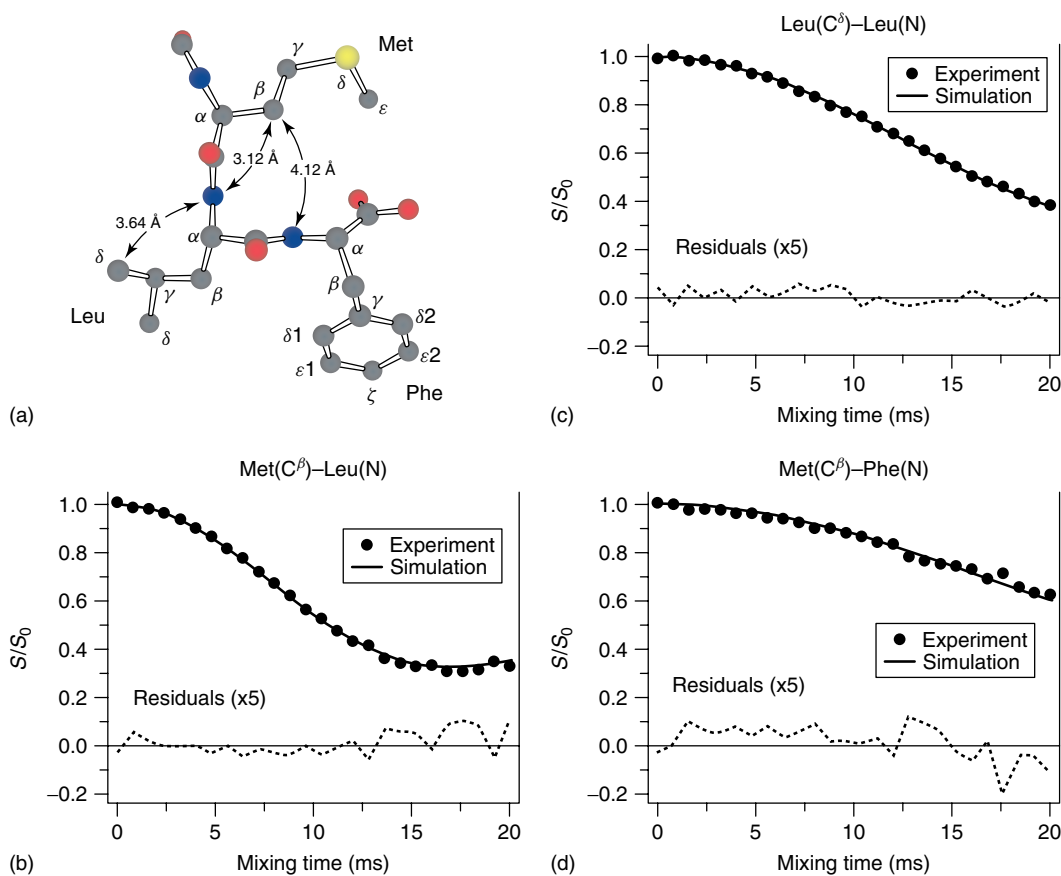


**Figure 6** Representative frequency-selective REDOR measurements of  $^{13}\text{C}$ - $^{15}\text{N}$  distances in formyl- $U$ - $^{13}\text{C}$ ,  $^{15}\text{N}$ -Met-Leu-Phe.<sup>76,111</sup> (a) Structural model of f-MLF based on the published X-ray structure of the methyl ester analog, f-MLF-OMe<sup>114</sup> (no X-ray structure is available for f-MLF), displaying the distances determined in panels (b)–(d). Experimental FS-REDOR  $S/S_0$  curves and simulations are shown for (b) Met( $C\beta$ )-Leu(N), (c) Leu( $C\delta$ )-Leu(N), and (d) Met( $C\beta$ )-Phe(N), and correspond to distances of  $3.12 \pm 0.03$ ,  $3.64 \pm 0.09$ , and  $4.12 \pm 0.15$  Å, respectively. Data were recorded at 500 MHz  $^1\text{H}$  frequency and 10.0 kHz MAS rate. For the measurements shown, resonant frequency-selective Gaussian pulses of 2 ms (Met  $^{13}\text{C}\beta$ ), 4 ms (Leu  $^{13}\text{C}\delta$ ), and 10 ms (Leu or Phe  $^{15}\text{N}$ ) were used to selectively recouple appropriate spin pairs. The measurements were performed in a sample prepared by cocrystallizing f- $U$ - $^{13}\text{C}$ ,  $^{15}\text{N}$ -MLF with natural abundance f-MLF in a 1:9 ratio, to minimize the interference from intermolecular  $^{13}\text{C}$ - $^{15}\text{N}$  couplings. (Reproduced from Ref. 111. © The National Academy of Sciences of the USA, 2002.)

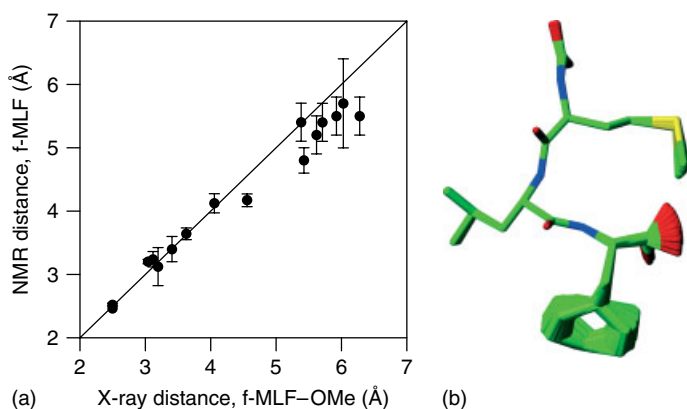


**Figure 7** (a) Comparison of  $^{13}\text{C}$ - $^{15}\text{N}$  distances in formyl- $U$ - $^{13}\text{C}$ ,  $^{15}\text{N}$ -Met-Leu-Phe measured by using frequency-selective REDOR<sup>76,111</sup> with the corresponding X-ray distances in f-MLF-OMe.<sup>114</sup> The uncertainties in NMR distances correspond to  $\pm 2\sigma$ . (b) Representative subset of f-MLF structures (PDB entry 1Q7O) calculated on the basis of SSNMR torsion angle and FS-REDOR  $^{13}\text{C}$ - $^{15}\text{N}$  distance restraints. (Reproduced from Ref. 111. © The National Academy of Sciences of the USA, 2002.)

times ( $\tau_{\text{mix}} \geq \sim 10\text{--}15$  ms), as well as significant lineshape perturbations caused by the refocusing of antiphase coherences into observable  $^{13}\text{C}$  magnetization during detection.<sup>75</sup> Although several extensions of the REDOR technique that can report on the different  $^{13}\text{C}\text{--}^{15}\text{N}$  dipolar couplings present in multispin systems have been proposed,<sup>103–108</sup> these schemes are not generally applicable to U- $^{13}\text{C}$ ,  $^{15}\text{N}$  peptides and proteins – this is primarily related to the fact that most of these experiments involve the application of  $180^\circ$  pulse trains on the  $^{13}\text{C}$  channel, which would also reintroduce the large  $\sim 2$  kHz one-bond  $^{13}\text{C}\text{--}^{13}\text{C}$  dipolar couplings that are normally efficiently averaged by rapid MAS.<sup>109,110</sup>

In this section, we discuss several recently developed SSNMR techniques that alleviate the aforementioned problems and facilitate the accurate and precise measurements of multiple weak heteronuclear  $^{13}\text{C}\text{--}^{15}\text{N}$  dipolar couplings in U- $^{13}\text{C}$ ,  $^{15}\text{N}$  labeled molecules. These techniques are based on the highly experimentally robust REDOR scheme discussed in the section “Rotational Echo Double Resonance”. Although REDOR does not formally suppress homonuclear dipolar couplings between the irradiated  $^{15}\text{N}$  spins as noted in the section “Symmetry-based Pulse Sequences”, this effect can be safely neglected when considering the evolution of  $^{13}\text{C}$  magnetization for U- $^{13}\text{C}$ ,  $^{15}\text{N}$  enriched polypeptides, where typical  $^{15}\text{N}\text{--}^{15}\text{N}$  dipolar couplings are small,  $b_{\text{NN}}/2\pi < 50$  Hz, and the amide  $^{15}\text{N}$  nuclei resonate in a relatively narrow frequency range. Moreover, since the basic principles behind these new techniques are quite general, alternate implementations employing pulse sequences that generate an analogous REDOR-like effective heteronuclear dipolar Hamiltonian,  $\overline{H}_D^{(0)} \propto \hat{I}_{1z}\hat{I}_{2z}$  (e.g., SPI-R<sup>3</sup> or the appropriate symmetry-based schemes), can also be readily envisioned.

#### 4.1 Frequency-Selective REDOR

The effective Hamiltonian describing the spin–spin couplings within a system of  $n$   $^{13}\text{C}$  spins and  $m$   $^{15}\text{N}$  spins during the REDOR pulse sequence can be written:

$$\overline{H} = \sum_{i=1}^n \sum_{j=1}^m \tilde{\omega}_{ij}^D 2\hat{C}_{iz}\hat{N}_{jz} + \sum_{i<j} \pi J_{ij} 2\hat{C}_{iz}\hat{C}_{jz} \quad (39)$$

where operators  $\hat{C}$  and  $\hat{N}$  represent  $^{13}\text{C}$  and  $^{15}\text{N}$  spins, respectively,  $J_{ij}$  is the  $^{13}\text{C}\text{--}^{13}\text{C}$  J-coupling constant and the expression for  $\tilde{\omega}_{ij}^D$ , assuming that the principal axis frame for each interaction coincides with the crystallite-fixed frame, is given in equation (31). The evolution of transverse magnetization for the  $i$ th  $^{13}\text{C}$  spin (i.e.,  $\hat{\rho}(0) = \hat{C}_{ix}$ ) under this effective Hamiltonian yields the observable powder-averaged signal:

$$S(\tau_{\text{mix}}) = \left\langle \prod_j \cos(\tilde{\omega}_{ij}^D \tau_{\text{mix}}) \right\rangle \prod_{j \neq i} \cos(\pi J_{ij} \tau_{\text{mix}}) \quad (40)$$

Since the observable  $^{13}\text{C}$  coherences evolve simultaneously as products of cosine terms involving all relevant spin–spin couplings, the strongest couplings tend to dominate the evolution making the accurate quantification of weak heteronuclear dipolar couplings virtually impossible.

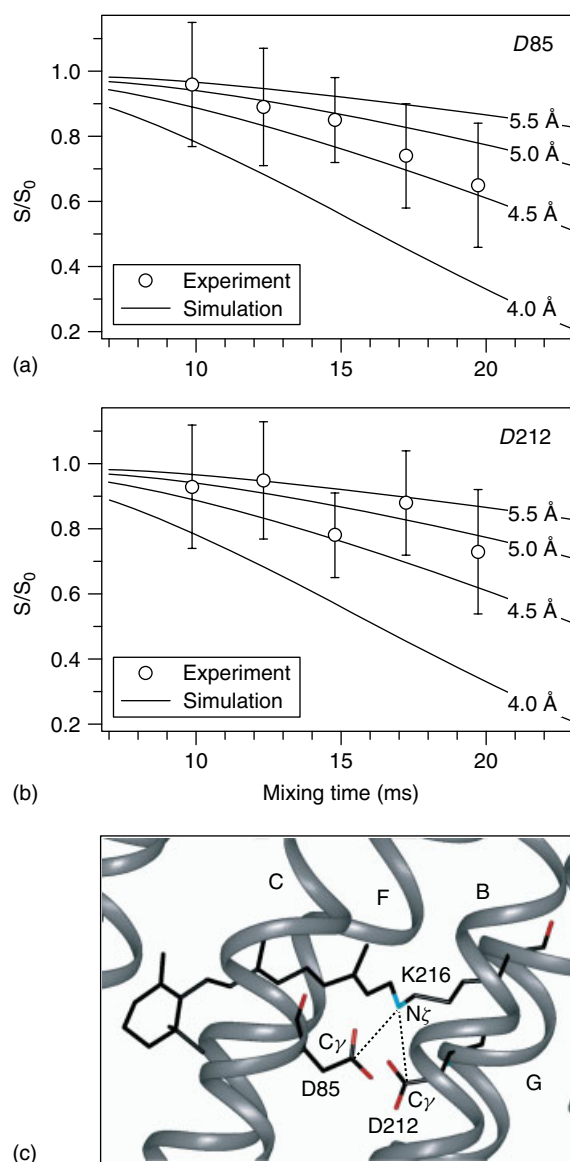


**Figure 8** Frequency-selective REDOR distance measurements from the Schiff base (Lys-216N $\zeta$ ) to (a) Asp-85 C $\gamma$  and (b) Asp-212 C $\gamma$  in light-adapted U- $^{13}\text{C}$ ,  $^{15}\text{N}$  labeled bacteriorhodopsin. Spectra were recorded at 317 MHz  $^1\text{H}$  frequency and 6.5 kHz MAS rate; the total experiment duration was  $\sim 10$  days. The best-fit distances extracted from the experimental FS-REDOR  $S/S_0$  trajectories are  $4.7 \pm 0.3$  Å for Asp-85 and  $4.9 \pm 0.5$  Å for Asp-212 – the corresponding distances in several X-ray structures of bR (PDB entries 1BRR,<sup>117</sup> 1QHI,<sup>118</sup> and 1C3W<sup>119</sup>) are in the range 4.3–5.0 Å for Asp-85 and 4.0–4.4 Å for Asp-212. (c) Structural model of the bR active site based on X-ray diffraction studies, showing  $\alpha$ -helices B, C, F, and G, the chromophore (comprising retinal with its Schiff base linkage to Lys-216), and the Asp-85 and Asp-212 side chains. The distances between the Schiff base  $^{15}\text{N}$  and Asp  $^{13}\text{C}\gamma$ , measured by FS-REDOR, are indicated by dotted lines. (Adapted from Ref. 115. © American Chemical Society, 2001.)

Given that the effective Hamiltonian in equation (39) is a sum of commuting bilinear terms, it can be refocused by using spin-echo techniques. This idea forms the basis for the frequency-selective rotational echo double resonance (FS-REDOR) scheme<sup>75,76</sup> shown in Figure 5. FS-REDOR consists of a pair of rotor-synchronized, frequency-selective

(e.g., Gaussian-shaped)  $180^\circ$  pulses applied simultaneously on the  $^{13}\text{C}$  and  $^{15}\text{N}$  channels and bracketed by two identical REDOR periods, of length  $\tau_{\text{mix}}/2$  each, during which all  $^{13}\text{C}$ – $^{15}\text{N}$  dipolar and  $^{13}\text{C}$ – $^{13}\text{C}$  J-couplings evolve. Assuming that the selective  $180^\circ$  pulses are applied at frequencies of spins  $C_k$  and  $N_l$ , the effective Hamiltonian for the entire pulse sequence that is relevant to the evolution of spin  $C_k$  is given by

$$\overline{\hat{H}} = \tilde{\omega}_{kl}^D 2\hat{C}_{kz}\hat{N}_{lz} \quad (41)$$

leading to the observable  $C_k$  signal, which is equivalent to that expected for conventional REDOR for an isolated  $^{13}\text{C}$ – $^{15}\text{N}$  spin pair:

$$S(\tau_{\text{mix}}) = \langle \hat{C}_{kx} \rangle(\tau_{\text{mix}}) = \langle \cos(\tilde{\omega}_{kl}^D \tau_{\text{mix}}) \rangle \quad (42)$$

These results imply that within a system of many coupled  $^{13}\text{C}$  and  $^{15}\text{N}$  nuclei it is, in principle, possible to isolate a single  $^{13}\text{C}$ – $^{15}\text{N}$  dipolar coupling of interest and suppress all other  $^{13}\text{C}$ – $^{15}\text{N}$  dipolar interactions as well as  $^{13}\text{C}$ – $^{13}\text{C}$  J-couplings, provided that the chemical shifts of the relevant  $^{13}\text{C}$  and  $^{15}\text{N}$  spins are such that they can be irradiated in a frequency-selective manner. In practice, bandwidths in the  $\pm 2000$  to  $\pm 200$  Hz regime have been obtained for 1–10 ms Gaussian-shaped pulses.<sup>76</sup> Note also that the selectivity of the FS-REDOR experiment can potentially be tuned further by using longer, weaker pulses with different shapes, albeit with an accompanying loss in spectral sensitivity due to transverse  $^{13}\text{C}$  relaxation.

The FS-REDOR technique and extensions thereof have been successfully applied to several U- $^{13}\text{C}$ ,  $^{15}\text{N}$  enriched amino acids and peptides,<sup>76,111–113</sup> including the detection of a critical salt bridge between the side chains of residues Asp-23 and Lys-28 in Alzheimer's  $\beta$ -amyloid fibrils.<sup>112</sup> In Figure 6, we show several representative FS-REDOR measurements of  $^{13}\text{C}$ – $^{15}\text{N}$  dipolar couplings (corresponding to distances in the  $\sim 3$ – $4$  Å regime) for a three-residue peptide, formyl-U- $^{13}\text{C}$ ,  $^{15}\text{N}$ -Met-Leu-Phe (see spectra in Figure 1a). These data clearly indicate that multiple  $^{13}\text{C}$ – $^{15}\text{N}$  dipolar couplings and  $^{13}\text{C}$ – $^{13}\text{C}$  J-couplings, that would normally significantly perturb the REDOR dephasing trajectories, are efficiently suppressed by FS-REDOR – notably, markedly different dipolar dephasing trajectories are obtained for the Met( $C\beta$ ) site by simply changing the frequency of the

$^{15}\text{N}$  selective pulse from Leu(N) (Figure 6b) to Phe(N) (Figure 6d), and both trajectories are completely free of the effects of the large  $\sim 200$  Hz two-bond Met( $C\beta$ )–Met(N) coupling. Altogether, FS-REDOR measurements in f-MLF have enabled the quantitative determination of 16  $^{13}\text{C}$ – $^{15}\text{N}$  distances between  $\sim 2.5$  and  $6$  Å, with typical precision ( $2\sigma$ ) of  $\sim 0.1$ – $0.3$  Å. The  $^{13}\text{C}$ – $^{15}\text{N}$  distances determined by SSNMR were generally found to be in good agreement with the corresponding distances obtained using X-ray diffraction for the methyl ester analog of f-MLF<sup>114</sup> as illustrated in Figure 7(a) (note that no X-ray structure is available for f-MLF). Indeed, in combination with a set of backbone and side-chain torsion angle restraints, the FS-REDOR  $^{13}\text{C}$ – $^{15}\text{N}$  distance restraints were used to determine a high-resolution SSNMR structure for f-MLF<sup>111</sup> (Figure 7b).

While the applications of FS-REDOR to the structural studies of small U- $^{13}\text{C}$ ,  $^{15}\text{N}$  enriched peptides (or larger systems, segmentally labeled with U- $^{13}\text{C}$ ,  $^{15}\text{N}$  amino acids) displaying well-resolved  $^{13}\text{C}$  and  $^{15}\text{N}$  spectra are relatively straightforward, analogous studies of larger U- $^{13}\text{C}$ ,  $^{15}\text{N}$  labeled proteins are typically considerably more challenging owing to increased spectral crowding. Nevertheless, in certain cases where the resonances of primary interest are sufficiently well resolved, FS-REDOR techniques can be extended to address interesting structural questions in such systems.<sup>115,116</sup> Figure 8 illustrates an application of this type, where FS-REDOR was used to determine long-range ( $\sim 4$ – $5$  Å) distances between the  $^{13}\text{C}\gamma$  side-chain carbons of two aspartic acid residues and a Schiff base  $^{15}\text{N}$  in the active site of a 26 kDa U- $^{13}\text{C}$ ,  $^{15}\text{N}$  labeled integral membrane protein, bacteriorhodopsin (bR).<sup>115</sup> This FS-REDOR experiment in bR was facilitated by the fact that the Schiff base  $^{15}\text{N}$  has a unique chemical shift of  $\sim 165$  ppm in the light-adapted form of the protein (i.e.,  $\sim 30$ – $60$  ppm downfield of backbone amide resonances), and that  $\text{C}\gamma$  signals for the Asp-85 and Asp-212 residues of interest are relatively well resolved from each other as well as from  $\text{C}\gamma$  resonances arising from the remaining Asp residues.

## 4.2 3-D TEDOR Techniques

A more general approach toward the simultaneous measurement of multiple heteronuclear  $^{13}\text{C}$ – $^{15}\text{N}$  dipolar couplings in U- $^{13}\text{C}$ ,  $^{15}\text{N}$  labeled polypeptides with arbitrary  $^{13}\text{C}$  and  $^{15}\text{N}$  chemical shifts is based on multidimensional heteronuclear

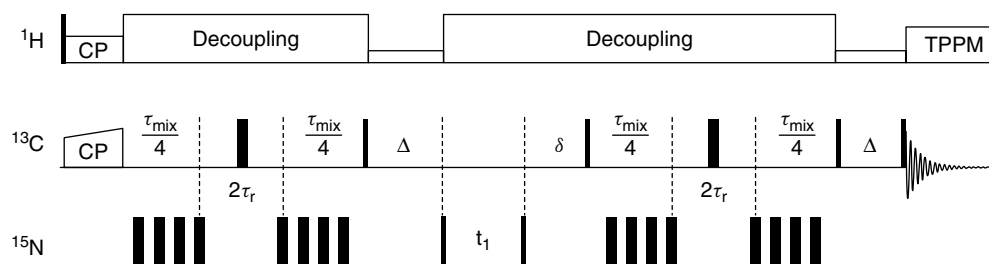


**Figure 9** 3-D  $z$ -filtered TEDOR (ZF-TEDOR) pulse sequence.<sup>78</sup> Narrow and wide black rectangles correspond to  $90^\circ$  and  $180^\circ$  pulses. The delay  $\delta$  ensures that the total delay between the REDOR dipolar mixing periods is equal to an integer number of rotor cycles, which is required for the efficient reconversion of  $^{13}\text{C}$ – $^{15}\text{N}$  antiphase coherences into observable  $^{13}\text{C}$  magnetization. The  $z$ -filter periods  $\Delta$  eliminate undesirable multiple quantum and antiphase spin coherences generated by  $^{13}\text{C}$ – $^{13}\text{C}$  J-evolution – in the studies discussed here, the  $z$ -filter periods were of minimum duration ( $\Delta = 200$   $\mu\text{s}$ ) and utilized a weak RF field applied concurrently on the  $^1\text{H}$  channel ( $\omega_{\text{RF}} \approx \omega_r$ ) to rapidly dephase transverse  $^{13}\text{C}$  spin coherences. However, alternate  $z$ -filter implementations can also be employed<sup>79,122</sup>

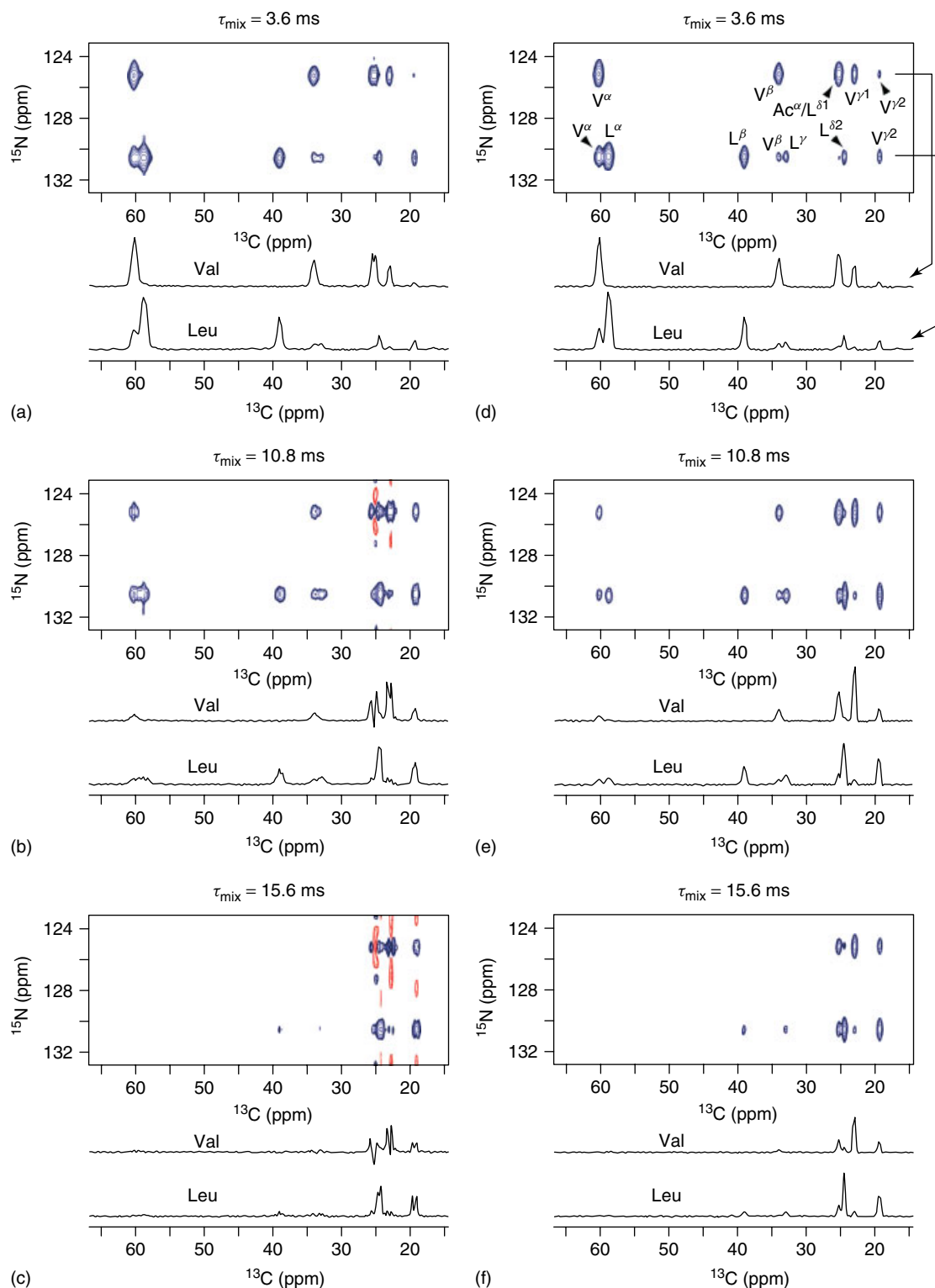


**Figure 10** Representative 2-D planes from 3-D TEDOR experiments in U- $^{13}\text{C}$ ,  $^{15}\text{N}$  labeled acetyl-Val-Leu corresponding to dipolar mixing times of 3.6, 10.8, and 15.6 ms. Spectra were recorded at 500 MHz  $^1\text{H}$  frequency and 10.0 kHz MAS rate, using the pulse scheme in Figure 9 implemented without (a)–(c) or with (d)–(f) z-filter delays. Positive and negative contours are shown in blue and red, respectively. These spectra demonstrate that the use of z-filters in 3-D TEDOR experiments performed on U- $^{13}\text{C}$ ,  $^{15}\text{N}$  labeled molecules eliminates the detrimental effects of  $^{13}\text{C}$ – $^{13}\text{C}$  J-couplings and leads to pure absorption-mode spectra. (Adapted from Ref. 78. © American Chemical Society, 2002.)

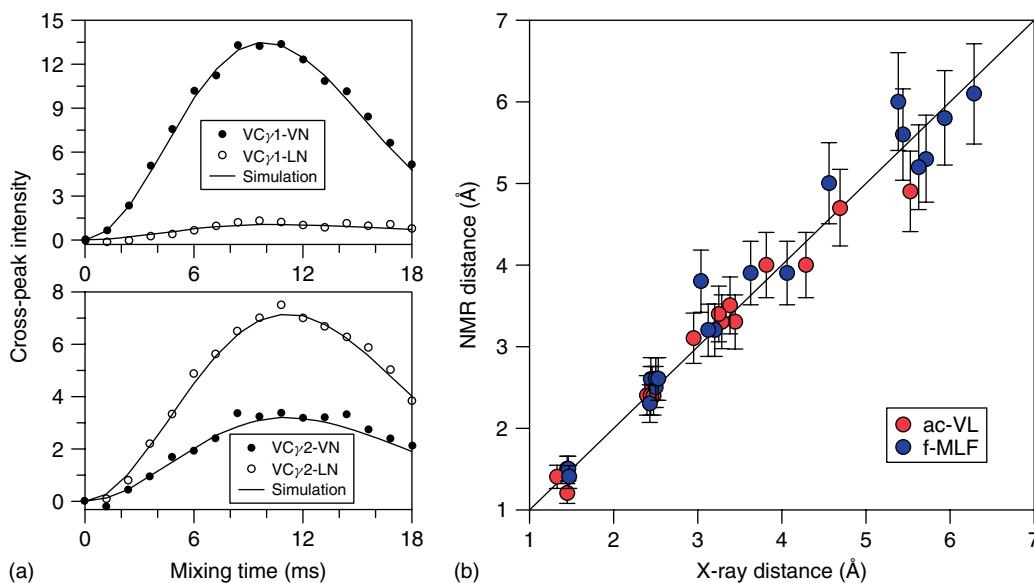


**Figure 11** (a) Representative 3-D ZF-TEDOR cross-peak buildup trajectories for U- $^{13}\text{C}$ ,  $^{15}\text{N}$ -acetyl-Val-Leu, reporting on the dipolar couplings between Val  $^{13}\text{C}\gamma 1$  or  $^{13}\text{C}\gamma 2$  and Val  $^{15}\text{N}$  or Leu  $^{15}\text{N}$ . The  $^{13}\text{C}$ - $^{15}\text{N}$  distances extracted from the trajectories are as follows: Val( $\text{C}\gamma 1$ )-Val(N): 3.1 Å; Val( $\text{C}\gamma 1$ )-Leu(N): 4.7 Å; Val( $\text{C}\gamma 2$ )-Val(N): 4.0 Å; Val( $\text{C}\gamma 2$ )-Leu(N): 3.5 Å (Reproduced from Ref. 78. © American Chemical Society, 2002). (b) Comparison of  $^{13}\text{C}$ - $^{15}\text{N}$  distances in U- $^{13}\text{C}$ ,  $^{15}\text{N}$ -acetyl-Val-Leu and formyl-U- $^{13}\text{C}$ ,  $^{15}\text{N}$ -Met-Leu-Phe measured by using 3-D ZF-TEDOR<sup>78</sup> with the corresponding X-ray distances (f-MLF X-ray distances refer to f-MLF-OMe, cf. Figures 6 and 7). Uncertainties in the NMR distances correspond to  $\pm 10\%$  of the measured distance (see Ref. 78 for a detailed discussion). Note that U- $^{13}\text{C}$ ,  $^{15}\text{N}$  labeled ac-VL and f-MLF peptides used in this study were diluted in a 1:4 and 1:9 ratio, respectively, in corresponding natural abundance peptides, to minimize the effects of intermolecular  $^{13}\text{C}$ - $^{15}\text{N}$  couplings

correlation (HETCOR) spectroscopy. In the simplest implementation of a 3-D HETCOR scheme, a series of 2-D  $^{15}\text{N}$ - $^{13}\text{C}$  chemical shift correlation spectra are acquired as a function of a  $^{15}\text{N}$ - $^{13}\text{C}$  dipolar magnetization transfer (or mixing) period – note, however, that an additional chemical shift dimension can also be readily incorporated into these schemes for increased spectral resolution.<sup>79</sup> Consequently, for each resolved  $^{13}\text{C}$  site,  $C_i$ , cross peaks located at frequencies  $(\Omega_{N_j}, \Omega_{C_i})$  with  $j = 1, 2, \dots$  are observed in the 2-D spectra for  $C_i$ - $N_j$  pairs exhibiting sufficiently strong dipolar couplings – more importantly, in the context of quantitative measurements, the information about  $C_i$ - $N_j$  distances is encoded in the full cross-peak buildup trajectories recorded as a function of the mixing time.

Several 3-D  $^{15}\text{N}$ - $^{13}\text{C}$  HETCOR schemes based on REDOR mixing and  $90^\circ$   $^{13}\text{C}$  and  $^{15}\text{N}$  magnetization transfer pulses have been proposed<sup>77–79,120</sup> on the basis of the original TEDOR sequences developed by Schaefer and coworkers.<sup>80,121</sup> Of these 3-D TEDOR experiments, the “out-and-back” type schemes with  $^{13}\text{C}$  detection, that avoid the recoupling of  $^{13}\text{C}$ - $^{13}\text{C}$  dipolar interactions by minimizing the RF irradiation on the  $^{13}\text{C}$  channel are the most promising for applications to U- $^{13}\text{C}$ ,  $^{15}\text{N}$  labeled molecules.<sup>77–79</sup> In addition, for measurements of weak  $^{13}\text{C}$ - $^{15}\text{N}$  couplings requiring relatively long mixing times, these schemes must be compensated for spectral artifacts caused by homonuclear  $^{13}\text{C}$ - $^{13}\text{C}$  J-evolution. One such scheme, shown in Figure 9 and referred to as 3-D ZF-TEDOR,<sup>78</sup> employs two  $z$ -filter periods to suppress undesirable antiphase and multiple quantum coherences generated by the evolution of transverse  $^{13}\text{C}$  magnetization under one-bond  $^{13}\text{C}$ - $^{13}\text{C}$  J-couplings. The importance of eliminating these undesirable  $^{13}\text{C}$  coherences

is illustrated in Figure 10 for a model dipeptide, U- $^{13}\text{C}$ ,  $^{15}\text{N}$ -acetyl-Val-Leu (ac-VL). Specifically, in the absence of the  $z$ -filter periods spurious cross peaks and phase-twisted lineshapes are observed in the 2-D  $^{15}\text{N}$ - $^{13}\text{C}$  spectra, particularly for longer mixing times (Figure 10(a)–(c)), which precludes the accurate determination of the actual cross-peak positions and intensities. On the other hand, the insertion of  $z$ -filters as indicated in Figure 9 restores pure absorption-mode correlation spectra that can be readily analyzed for all mixing times (Figure 10(d)–(f)).

The spectra in Figure 10(d)–(f) illustrate the utility of 3-D ZF-TEDOR for simultaneously detecting multiple structurally interesting  $^{13}\text{C}$ - $^{15}\text{N}$  dipolar couplings in U- $^{13}\text{C}$ ,  $^{15}\text{N}$  enriched biomolecules. For example, the relative intensities of correlations between valine  $\text{C}\gamma 1$  and  $\text{C}\gamma 2$  and both amide  $^{15}\text{N}$  sites obtained for different mixing times immediately provide valuable qualitative information about the rotameric state of the side chain for that residue. Quantitative estimates of the  $^{13}\text{C}$ - $^{15}\text{N}$  distances can be obtained by monitoring the complete cross-peak buildup trajectories, with the  $C_i$ - $N_j$  cross-peak intensity as a function of  $\tau_{\text{mix}}$  given by

$$I_{ij}(\tau_{\text{mix}}) = \Lambda_i e^{-\Gamma_i \tau_{\text{mix}}} \left\langle \sin^2 \left( \frac{\tilde{\omega}_{ij}^D \tau_{\text{mix}}}{2} \right) \times \prod_{k \neq j} \cos^2 \left( \frac{\tilde{\omega}_{ik}^D \tau_{\text{mix}}}{2} \right) \right\rangle \prod_{l \neq i} \cos^2(\pi J_{il} \tau_{\text{mix}}/2) \quad (43)$$

where  $\Lambda_i$  is the cross-peak amplitude scaling factor, and  $\Gamma_i$  is the relaxation rate constant for  $C_i$  spin coherences.

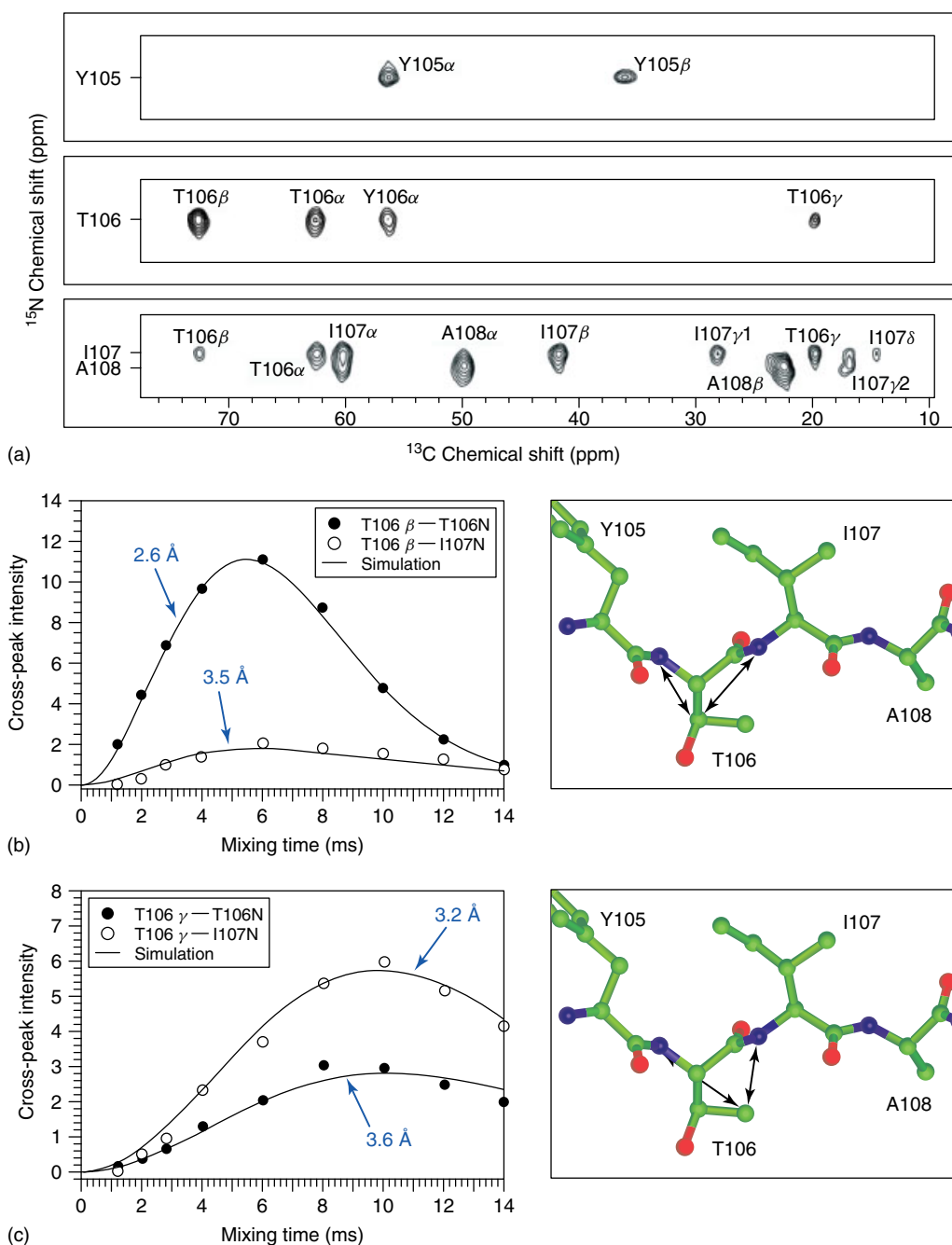


**Figure 12** Representative 3-D ZF-TEDOR  $^{13}\text{C}$ - $^{15}\text{N}$  distance measurements for transthyretin 105–115 (amino acid sequence YTIAALLSPYS) amyloid fibrils, containing a U- $^{13}\text{C}$ ,  $^{15}\text{N}$  labeled four-residue stretch Y105–A108. (a) Strips from a 2-D  $^{15}\text{N}$ - $^{13}\text{C}$  correlation spectrum recorded with a mixing time  $\tau_{\text{mix}} = 6.0$  ms. Resonance assignments are based on Ref. 124. (b) Experimental and simulated trajectories for the T106(C $\beta$ )-T106(N) and T106(C $\beta$ )-I107(N) cross peaks as a function of the dipolar mixing time, and the relevant molecular fragment displaying the measured distances. (c) Same as panel (b) but for T106(C $\gamma$ ). (Reproduced from Ref. 125. © The National Academy of Sciences of the USA, 2004.)

While 3-D TEDOR-type schemes simultaneously restore the dipolar couplings between a given  $^{13}\text{C}$  spin and all nearby  $^{15}\text{N}$  nuclei, the cross-peak buildup trajectories are found to be determined primarily by the active dipolar coupling responsible for the appearance of the cross peak at frequencies ( $\Omega_{\text{mathrm}N_j}$ ,  $\Omega_{C_i}$ ) in the 2-D spectra and represented by the sine squared term in equation (43). Moreover, although 3-D ZF-TEDOR suppresses most of the detrimental  $^{13}\text{C}$ - $^{13}\text{C}$  J-evolution effects, the cross-peak intensities are still modulated

by  $^1J_{\text{CC}}$ , which reduces the spectral sensitivity and, in practice, restricts the useful  $^{15}\text{N}$ - $^{13}\text{C}$  mixing times to  $\tau_{\text{mix}} \sim 8$ –14 ms depending on the value of  $^1J_{\text{CC}}$ . Finally, we note that the cross-peak buildup trajectories exhibit a formal dependence on the relative orientations of the active and passive  $^{13}\text{C}$ - $^{15}\text{N}$  dipolar couplings – this is somewhat problematic since the relative dipolar tensor orientations are generally unknown and to include them as fit parameters would be impractical. Fortunately, it is possible to use instead a simple analytical



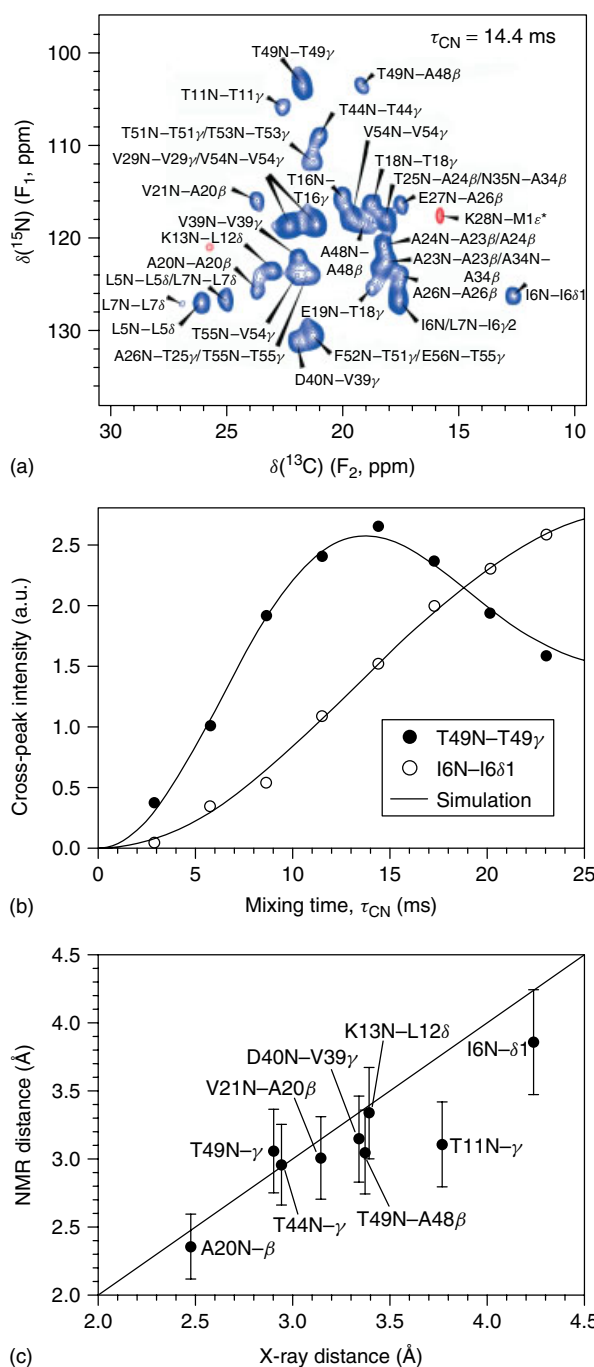
**Figure 13** High-resolution three-dimensional structure of transthyretin 105–115 in amyloid fibrils determined using MAS SSNMR techniques (PDB entry 1RVS).<sup>125</sup> The structure was determined using 76 experimental restraints, recorded primarily on three peptide samples that were U-<sup>13</sup>C,<sup>15</sup>N labeled in overlapping stretches of four residues: Y105–A108, A108–L111, and L111–Y114. The experimental restraints included 35 <sup>13</sup>C–<sup>15</sup>N distances in the ~2.5–6 Å regime determined mostly using 3-D ZF-TEDOR, and 41 backbone torsion angle restraints (on 19  $\phi$  and  $\psi$  angles) based on dipolar tensor correlation techniques and isotropic chemical shifts

model based on Bessel function expansions of REDOR NMR signals<sup>123</sup> that depends only on the dipolar coupling magnitudes and is completely free of geometric parameters. According to this model, the  $C_i$ – $N_j$  cross-peak intensity as a function of  $\tau_{\text{mix}}$  can be approximated as<sup>78</sup>

$$I_{ij}(\tau_{\text{mix}}) \approx \Lambda_i e^{-\Gamma_i \tau_{\text{mix}}} \{1 - [J_0(\sqrt{2}b_{ij} \tau_{\text{mix}}/2\pi)]^2\} \times \prod_{k \neq j} \{1 + [J_0(\sqrt{2}b_{ik} \tau_{\text{mix}}/2\pi)]^2\} \times \prod_{l \neq i} \cos^2(\pi J_{il} \tau_{\text{mix}}/2) \quad (44)$$

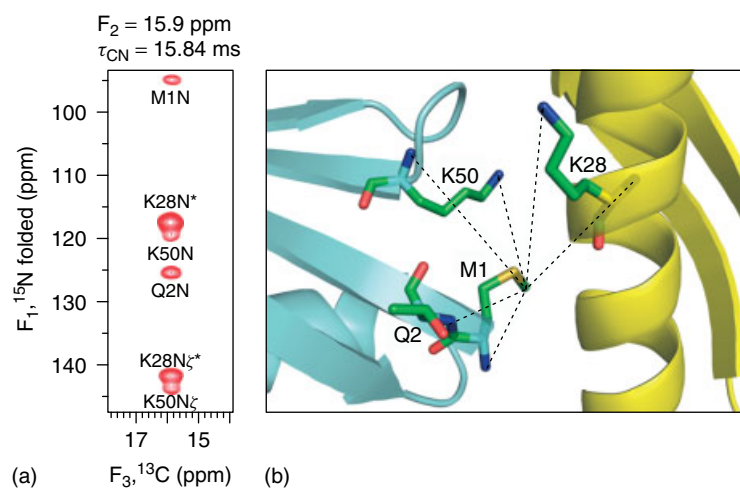
where  $J_0(x)$  is a Bessel function of zeroth order. For spin systems exhibiting highly resolved spectra all cross-peak trajectories corresponding to a given <sup>13</sup>C site can be fit simultaneously with a set of expressions similar to equation (44), which reduces the number of independent fit parameters and results in highest quality fits<sup>78</sup> – however, given that the most important features of the cross-peak buildup trajectories are primarily determined by the active dipolar coupling, in systems exhibiting more significant spectral overlap, individual trajectories can be modeled as discussed in Ref. 79. Finally, we note that the use of this approximate analytical model, as opposed to the analytical AHT result given in equation (43), is generally expected to be the major source of error in the measurements of <sup>13</sup>C–<sup>15</sup>N distances in the 3–5 Å regime, with typical uncertainties on the order of ~10–15% of the measured distance.<sup>78</sup>

Figure 11(a) shows representative experimental and simulated 3-D ZF-TEDOR trajectories for ac-VL. These data illustrate that <sup>13</sup>C–<sup>15</sup>N dipolar couplings corresponding to distances up to ~5 Å can be readily determined using this method, and that the simulation model in equation (44) provides a reasonable description of the experimental cross-peak buildup trajectories. In Figure 11(b), all <sup>13</sup>C–<sup>15</sup>N distances measured in ac-VL and f-MLF by using 3-D ZF-TEDOR<sup>78</sup> are compared with the corresponding X-ray diffraction distances – overall, the two sets of distances show a remarkably high degree of agreement. To demonstrate an application of 3-D ZF-TEDOR to a more challenging biological system, in Figure 12, we show representative spectra, as well as the experimental and simulated cross-peak buildup trajectories for a



**Figure 14** (a) 2-D slice from a 3-D SCT-TEDOR experiment on protein GB1 corresponding to the <sup>15</sup>N–<sup>13</sup>C<sup>methyl</sup> chemical shift correlation spectrum recorded with a dipolar mixing time 14.4 ms. Positive and negative cross peaks are drawn in blue and red, respectively. (b) Representative trajectories of cross-peak intensity as a function of the mixing time for T49N–T49 $\gamma$  and I6N–I6 $\delta$ 1 cross peaks, corresponding to <sup>15</sup>N–<sup>13</sup>C distances in the ~3–4 Å range. Best-fit simulations using an analytical model are also shown (–). (c) Comparison of selected <sup>15</sup>N–<sup>13</sup>C distances in GB1 determined using X-ray diffraction and 3-D SCT-TEDOR. Error bars correspond to  $\pm 10\%$  of the measured distance. (Reproduced from Ref. 79. © American Institute of Physics, 2008.)

segmentally U-<sup>13</sup>C,<sup>15</sup>N labeled amyloidogenic peptide corresponding to residues 105–115 of transthyretin.<sup>124,125</sup> In fact,



**Figure 15** (a) Small ( $F_1, F_3$ )-region taken from the 3-D  $^{15}\text{N}-^{13}\text{C}^{\text{methyl}}-^{13}\text{C}$  correlation spectrum of protein GB1 at the  $M1\epsilon$  frequency in  $F_2$ , showing the correlations between  $M1\epsilon$  and the neighboring  $^{15}\text{N}$  nuclei. Six cross peaks were observed in this region and assigned on the basis of the GB1  $^{13}\text{C}$  and  $^{15}\text{N}$  chemical shifts,<sup>55</sup> combined with the analysis of published GB1 crystal structures.<sup>129</sup> The four intramolecular correlations correspond to dipolar contacts between  $M1\epsilon$  and  $M1\text{N}$  ( $\text{NH}_3^+$ ),  $Q2\text{N}$ ,  $K50\text{N}$ , and  $K50\text{N}\zeta$ , and the two remaining cross peaks (indicated by asterisks) have been assigned to intermolecular contacts with  $K28\text{N}$  and  $K28\text{N}\zeta$ . (b) Structural model of GB1 in the trigonal lattice (PDB entry 1PGB),<sup>129</sup> which qualitatively accounts for the observed cross-peak pattern, with the relevant  $M1\epsilon - \text{N}$  distances indicated by dotted lines. The neighboring GB1 molecules in the crystal lattice are shown in ribbon representation in cyan and yellow, and residues  $M1$ ,  $Q2$ ,  $K50$ , and  $K28$  are shown in stick representation (the atom-types for these residues are colored as follows: C = green, O = red, N = blue, S = yellow). (Reproduced from Ref. 79. © American Institute of Physics, 2008.)

these 3-D ZF-TEDOR distance measurements provided a set of critical restraints used to determine the high-resolution peptide structure in amyloid fibrils (Figure 13).<sup>125</sup>

Despite the  $^1J_{CC}$ -modulation of cross-peak intensities, which attenuates the spectral sensitivity and somewhat limits the range of accessible dipolar mixing times, the 3-D ZF-TEDOR scheme shown in Figure 9 and applied to  $U-^{13}\text{C}, ^{15}\text{N}$  labeled samples is highly useful owing to its ability to rapidly provide a large number of  $^{13}\text{C}-^{15}\text{N}$  distance restraints. In addition, several approaches have been proposed to suppress the  $^{13}\text{C}-^{13}\text{C}$  J-modulation of cross-peak intensities in 3-D TEDOR experiments, resulting in increased sensitivity and/or resolution spectra at the expense of the number of  $^{13}\text{C}-^{15}\text{N}$  dipolar couplings that can be simultaneously determined in a single experiment. These approaches include the use of (i) selective  $^{13}\text{C}$  refocusing pulses,<sup>78</sup> (ii) constant-time (CT)- or semiconstant-time (SCT)-type pulse sequence elements of duration  $\sim 1/|J_{CC}|$  to refocus the J-evolution,<sup>79</sup> and (iii) biosynthetic labeling schemes that yield proteins fully enriched with  $^{15}\text{N}$ , but  $^{13}\text{C}$ -labeled only at specific sites for different residues<sup>126,127</sup> – this type of “magnetic dilution” abolishes most one-bond  $^{13}\text{C}-^{13}\text{C}$  J-couplings and allows the 3-D ZF-TEDOR scheme to be applied with no additional modifications.<sup>128</sup> As an example of this type of methodology, Figures 14 and 15 show an application of 3-D and 4D SCT-TEDOR schemes to the determination of multiple distance restraints between amide  $^{15}\text{N}$  sites and side-chain  $^{13}\text{C}$  methyl groups of alanine, isoleucine, leucine, methionine, threonine, and valine residues in the 56-amino acid B1 immunoglobulin binding domain of protein G (GB1) in the microcrystalline phase.<sup>79</sup> Remarkably, these experiments provide both intra- and intermolecular  $^{13}\text{C}-^{15}\text{N}$  dipolar coupling restraints, which yield information about the side-chain dihedral angles and the packing of protein molecules within the crystal lattice.

## 5 CONCLUSIONS

Recent advances in MAS SSNMR instrumentation and methodology as well as sample-preparation protocols have facilitated the widespread studies of highly or uniformly  $^{13}\text{C}, ^{15}\text{N}$  enriched peptides and small to medium-sized proteins, including a number of important biological systems that pose significant challenges for traditional high-resolution techniques. Measurements of long-range (greater than  $\sim 3$  Å) internuclear distance restraints in these systems by using dipolar recoupling techniques have the capacity to provide site-specific atomic-level insights about their three-dimensional structure and intermolecular interactions. In this article, we discussed several recent REDOR-based heteronuclear dipolar recoupling methods, which are experimentally robust and straightforward to implement and analyze, and which enable the accurate and precise measurements of multiple, weak  $^{13}\text{C}-^{15}\text{N}$  dipolar couplings in  $U-^{13}\text{C}, ^{15}\text{N}$  enriched peptides and proteins. In addition to the specific applications highlighted here, a multitude of analogous applications of these and related methods to other biological systems can also be readily envisaged.

## 6 RELATED ARTICLES

Magic-Angle Spinning; Rotating Solids; Cross Polarization in Solids; Heteronuclear Decoupling in Solids; REDOR and TEDOR; Homonuclear Recoupling Schemes in MAS NMR; Symmetry-Based Pulse Sequences in Magic-Angle Spinning Solid-State NMR; Structure Determination of Solid Proteins Using MAS and Isotopic Enrichment.

## 7 REFERENCES

- E. R. Andrew, A. Bradbury, and R. G. Eades, *Nature*, 1959, **183**, 1802.
- I. J. Lowe, *Phys. Rev. Lett.*, 1959, **2**, 285.
- M. M. Maricq and J. S. Waugh, *J. Chem. Phys.*, 1979, **70**, 3300.
- A. Pines, M. G. Gibby, and J. S. Waugh, *J. Chem. Phys.*, 1973, **59**, 569.
- E. O. Stejskal, J. Schaefer, and J. S. Waugh, *J. Magn. Reson.*, 1977, **28**, 105.
- A. E. Bennett, C. M. Rienstra, M. Auger, K. V. Lakshmi, and R. G. Griffin, *J. Chem. Phys.*, 1995, **103**, 6951.
- A. Detken, E. H. Hardy, M. Ernst, and B. H. Meier, *Chem. Phys. Lett.*, 2002, **356**, 298.
- M. Ernst, *J. Magn. Reson.*, 2003, **162**, 1.
- M. Mehring, 'Principles of High Resolution NMR in Solids', Springer-Verlag: Berlin, 1983.
- E. R. Andrew, S. Clough, L. F. Farnell, T. A. Gledhill, and I. Roberts, *Phys. Lett.*, 1966, **21**, 505.
- D. P. Raleigh, M. H. Levitt, and R. G. Griffin, *Chem. Phys. Lett.*, 1988, **146**, 71.
- M. H. Levitt, D. P. Raleigh, F. Creuzet, and R. G. Griffin, *J. Chem. Phys.*, 1990, **92**, 6347.
- M. G. Colombo, B. H. Meier, and R. R. Ernst, *Chem. Phys. Lett.*, 1988, **146**, 189.
- A. E. Bennett, R. G. Griffin, and S. Vega, in 'NMR Basic Principles and Progress', ed. B. Blumich, Springer-Verlag: Berlin, 1994, Vol. 33, p 1.
- R. G. Griffin, *Nat. Struct. Biol.*, 1998, **5**, 508.
- S. Dusold and A. Sebald, *Annu. Rep. NMR Spectrosc.*, 2000, **41**, 185.
- B. J. Wylie and C. M. Rienstra, *J. Chem. Phys.*, 2008, **128**, 052207.
- M. J. Duer, 'Introduction to Solid-State NMR Spectroscopy', Blackwell Science: Oxford, 2004.
- T. Gullion and J. Schaefer, *J. Magn. Reson.*, 1989, **81**, 196.
- T. Gullion and J. Schaefer, *Adv. Magn. Reson.*, 1989, **13**, 57.
- D. M. Gregory, D. J. Mitchell, J. A. Stringer, S. Kiihne, J. C. Shiels, J. Callahan, M. A. Mehta, and G. P. Drobny, *Chem. Phys. Lett.*, 1995, **246**, 654.
- L. M. McDowell and J. Schaefer, *Curr. Opin. Struct. Biol.*, 1996, **6**, 624.
- S. O. Smith, K. Aschheim, and M. Groesbeek, *Q. Rev. Biophys.*, 1996, **29**, 395.
- R. Tycko, *Q. Rev. Biophys.*, 2006, **39**, 1.
- F. A. Kovacs, D. J. Fowler, G. J. Gallagher, and L. K. Thompson, *Concepts Magn. Reson.*, 2007, **30A**, 21.
- A. E. McDermott, F. Creuzet, R. G. Griffin, L. E. Zawadzke, Q. Z. Ye, and C. T. Walsh, *Biochemistry*, 1990, **29**, 5767.
- L. M. McDowell, C. A. Klug, D. D. Beusen, and J. Schaefer, *Biochemistry*, 1996, **35**, 5395.
- D. P. Weliky, A. E. Bennett, A. Zvi, J. Anglister, P. J. Steinbach, and R. Tycko, *Nat. Struct. Biol.*, 1999, **6**, 141.
- F. Creuzet, A. McDermott, R. Gebhard, Kvd. Hoef, M. B. Spijker-Assink, J. Herzfeld, J. Lugtenburg, M. H. Levitt, and R. G. Griffin, *Science*, 1991, **251**, 783.
- S. O. Smith, R. Jonas, M. Braiman, and B. J. Bormann, *Biochemistry*, 1994, **33**, 6334.
- B. Isaac, G. J. Gallagher, Y. S. Balazs, and L. K. Thompson, *Biochemistry*, 2002, **41**, 3025.
- J. R. Long, J. L. Dindot, H. Zebroski, S. Kiihne, R. H. Clark, A. A. Campbell, P. S. Stayton, and G. P. Drobny, *Proc. Natl. Acad. Sci. U S A*, 1998, **95**, 12083.
- P. T. Lansbury, P. R. Costa, J. M. Griffiths, E. J. Simon, M. Auger, K. J. Halverson, D. A. Kocisko, Z. S. Hendsch, T. T. Ashburn, R. G. S. Spencer, B. Tidor, and R. G. Griffin, *Nat. Mol. Biol.*, 1995, **2**, 990.
- T. L. S. Benzinger, D. M. Gregory, T. S. Burkoth, H. Miller-Auer, D. G. Lynn, R. E. Botto, and S. C. Meredith, *Proc. Natl. Acad. Sci. U S A*, 1998, **95**, 13407.
- F. Shewmaker, R. B. Wickner, and R. Tycko, *Proc. Natl. Acad. Sci. U S A*, 2006, **103**, 19754.
- K. Wüthrich, 'NMR of Proteins and Nucleic Acids', Wiley: New York, 1986.
- J. Cavanagh, W. J. Fairbrother, A. G. Palmer, M. Rance, and N. J. Skelton, 'Protein NMR Spectroscopy: Principles and Practice', Elsevier, Academic Press: San Diego, 2007.
- R. R. Ernst, G. Bodenhausen, and A. Wokaun, 'Principles of Nuclear Magnetic Resonance in One and Two Dimensions', Oxford University Press: Oxford, 1987.
- H. B. R. Cole, S. W. Sparks, and D. A. Torchia, *Proc. Natl. Acad. Sci. U S A*, 1988, **85**, 6362.
- A. McDermott, T. Polenova, A. Bockmann, K. W. Zilm, E. K. Paulsen, R. W. Martin, and G. T. Montelione, *J. Biomol. NMR*, 2000, **16**, 209.
- J. Pauli, B. van Rossum, H. Forster, H. J. M. de Groot, and H. Oschkinat, *J. Magn. Reson.*, 2000, **143**, 411.
- R. W. Martin and K. W. Zilm, *J. Magn. Reson.*, 2003, **165**, 162.
- A. E. McDermott, *Curr. Opin. Struct. Biol.*, 2004, **14**, 554.
- C. E. Hughes and M. Baldus, *Annu. Rep. NMR Spectrosc.*, 2005, **55**, 121.
- A. Bockmann, *Angew. Chem. Int. Ed.*, 2008, **47**, 6110.
- M. Hong and R. G. Griffin, *J. Am. Chem. Soc.*, 1998, **120**, 7113.
- C. M. Rienstra, M. Hohwy, M. Hong, and R. G. Griffin, *J. Am. Chem. Soc.*, 2000, **122**, 10979.
- M. Baldus, A. T. Petkova, J. Herzfeld, and R. G. Griffin, *Mol. Phys.*, 1998, **95**, 1197.
- J. J. Helmus, K. Surewicz, P. S. Nadaud, W. K. Surewicz, and C. P. Jaroniec, *Proc. Natl. Acad. Sci. U S A*, 2008, **105**, 6284.
- M. Baldus, *Prog. NMR Spectrosc.*, 2002, **41**, 1.
- S. K. Straus, *Philos. Trans. R. Soc. London, Ser. B*, 2004, **359**, 997.
- I. Schnell and H. W. Spiess, *J. Magn. Reson.*, 2001, **151**, 153.
- D. Huster, L. S. Xiao, and M. Hong, *Biochemistry*, 2001, **40**, 7662.
- M. Hong, X. L. Yao, K. Jakes, and D. Huster, *J. Phys. Chem. B*, 2002, **106**, 7355.
- W. T. Franks, D. H. Zhou, B. J. Wylie, B. G. Money, D. T. Graesser, H. L. Frericks, G. Sahota, and C. M. Rienstra, *J. Am. Chem. Soc.*, 2005, **127**, 12291.
- J. L. Lorieu and A. E. McDermott, *J. Am. Chem. Soc.*, 2006, **128**, 11505.
- J. L. Lorieu and A. E. McDermott, *Magn. Reson. Chem.*, 2006, **44**, 334.
- M. Hong, *J. Phys. Chem. B*, 2007, **111**, 10340.
- J. L. Lorieu, L. A. Day, and A. E. McDermott, *Proc. Natl. Acad. Sci. U S A*, 2008, **105**, 10366.
- X. Feng, Y. K. Lee, D. Sandström, M. Eden, H. Maisel, A. Sebald, and M. H. Levitt, *Chem. Phys. Lett.*, 1996, **257**, 314.

61. Y. Ishii, T. Terao, and M. Kainosho, *Chem. Phys. Lett.*, 1996, **256**, 133.
62. M. Hong, J. D. Gross, and R. G. Griffin, *J. Phys. Chem. B*, 1997, **101**, 5869.
63. P. R. Costa, J. D. Gross, M. Hong, and R. G. Griffin, *Chem. Phys. Lett.*, 1997, **280**, 95.
64. X. Feng, M. Eden, A. Brinkmann, H. Luthman, L. Eriksson, A. Gräslund, O. N. Antzutkin, and M. H. Levitt, *J. Am. Chem. Soc.*, 1997, **119**, 12006.
65. X. Feng, P. J. E. Verdegem, Y. K. Lee, D. Sandström, M. Edén, P. Bovee-Geurts, W. J. de Grip, J. Lugtenburg, H. J. M. de Groot, and M. H. Levitt, *J. Am. Chem. Soc.*, 1997, **119**, 6853.
66. M. Hong, J. D. Gross, C. M. Rienstra, R. G. Griffin, K. K. Kumashiro, and K. Schmidt-Rohr, *J. Magn. Reson.*, 1997, **129**, 85.
67. M. Hong, J. D. Gross, W. Hu, and R. G. Griffin, *J. Magn. Reson.*, 1998, **135**, 169.
68. B. Reif, M. Hohwy, C. P. Jaroniec, C. M. Rienstra, and R. G. Griffin, *J. Magn. Reson.*, 2000, **145**, 132.
69. C. M. Rienstra, M. Hohwy, L. J. Mueller, C. P. Jaroniec, B. Reif, and R. G. Griffin, *J. Am. Chem. Soc.*, 2002, **124**, 11908.
70. J. C. Lansing, M. Hohwy, C. P. Jaroniec, A. F. L. Creemers, J. Lugtenburg, J. Herzfeld, and R. G. Griffin, *Biochemistry*, 2002, **41**, 431.
71. V. Ladizhansky, M. Veshkort, and R. G. Griffin, *J. Magn. Reson.*, 2002, **154**, 317.
72. V. Ladizhansky, C. P. Jaroniec, A. Diehl, H. Oschkinat, and R. G. Griffin, *J. Am. Chem. Soc.*, 2003, **125**, 6827.
73. W. T. Franks, B. J. Wylie, S. A. Stellfox, and C. M. Rienstra, *J. Am. Chem. Soc.*, 2006, **128**, 3154.
74. W. T. Franks, B. J. Wylie, H. L. Schmidt, A. J. Nieuwkoop, R. M. Mayrhofer, G. J. Shah, D. T. Graesser, and C. M. Rienstra, *Proc. Natl. Acad. Sci. U S A*, 2008, **105**, 4621.
75. C. P. Jaroniec, B. A. Tounge, C. M. Rienstra, J. Herzfeld, and R. G. Griffin, *J. Am. Chem. Soc.*, 1999, **121**, 10237.
76. C. P. Jaroniec, B. A. Tounge, J. Herzfeld, and R. G. Griffin, *J. Am. Chem. Soc.*, 2001, **123**, 3507.
77. C. A. Michal and L. W. Jelinski, *J. Am. Chem. Soc.*, 1997, **119**, 9059.
78. C. P. Jaroniec, C. Filip, and R. G. Griffin, *J. Am. Chem. Soc.*, 2002, **124**, 10728.
79. J. J. Helmus, P. S. Nadaud, N. Hofer, and C. P. Jaroniec, *J. Chem. Phys.*, 2008, **128**, 052314.
80. A. W. Hing, S. Vega, and J. Schaefer, *J. Magn. Reson.*, 1992, **96**, 205.
81. T. Gullion, D. B. Baker, and M. S. Conradi, *J. Magn. Reson.*, 1990, **89**, 479.
82. T. Gullion and J. Schaefer, *J. Magn. Reson.*, 1991, **92**, 439.
83. A. Schmidt and S. Vega, *Isr. J. Chem.*, 1992, **32**, 215.
84. C. P. Jaroniec, B. A. Tounge, C. M. Rienstra, J. Herzfeld, and R. G. Griffin, *J. Magn. Reson.*, 2000, **146**, 132.
85. J. C. C. Chan and H. Eckert, *J. Magn. Reson.*, 2000, **147**, 170.
86. T. K. Weldeghiorghis and J. Schaefer, *J. Magn. Reson.*, 2003, **165**, 230.
87. N. Sinha, K. Schmidt-Rohr, and M. Hong, *J. Magn. Reson.*, 2004, **168**, 358.
88. M. E. Rose, *Elementary Theory of Angular Momentum*, Wiley: New York, 1957.
89. J. J. Sakurai, *Modern Quantum Mechanics*, Addison-Wesley: Redwood City, 1985.
90. T. G. Oas, R. G. Griffin, and M. H. Levitt, *J. Chem. Phys.*, 1988, **89**, 692.
91. M. H. Levitt, T. G. Oas, and R. G. Griffin, *Isr. J. Chem.*, 1988, **28**, 271.
92. U. Haeberlen and J. S. Waugh, *Phys. Rev.*, 1968, **175**, 453.
93. U. Haeberlen, *High-Resolution NMR in Solids: Selective Averaging*, Academic Press: New York, 1976.
94. N. C. Nielsen, H. Bildsøe, H. J. Jakobsen, and M. H. Levitt, *J. Chem. Phys.*, 1994, **101**, 1805.
95. M. Bak, J. T. Rasmussen, and N. C. Nielsen, *J. Magn. Reson.*, 2000, **147**, 296.
96. K. Takegoshi, K. Takeda, and T. Terao, *Chem. Phys. Lett.*, 1996, **260**, 331.
97. R. Fu, S. A. Smith, and G. Bodenhausen, *Chem. Phys. Lett.*, 1997, **272**, 361.
98. Y. K. Lee, N. D. Kurur, M. Helmle, O. G. Johannessen, N. C. Nielsen, and M. H. Levitt, *Chem. Phys. Lett.*, 1995, **242**, 304.
99. A. Brinkmann, M. Eden, and M. H. Levitt, *J. Chem. Phys.*, 2000, **112**, 8539.
100. A. Brinkmann and M. H. Levitt, *J. Chem. Phys.*, 2001, **115**, 357.
101. M. H. Levitt, *J. Chem. Phys.*, 2008, **128**, 052205.
102. J. C. C. Chan, *Chem. Phys. Lett.*, 2001, **335**, 289.
103. A. E. Bennett, L. R. Becerra, and R. G. Griffin, *J. Chem. Phys.*, 1994, **100**, 812.
104. A. E. Bennett, C. M. Rienstra, P. T. Lansbury, and R. G. Griffin, *J. Chem. Phys.*, 1996, **105**, 10289.
105. T. Gullion and C. H. Pennington, *Chem. Phys. Lett.*, 1998, **290**, 88.
106. O. Liivak and D. B. Zax, *J. Chem. Phys.*, 2000, **113**, 1088.
107. O. Liivak and D. B. Zax, *J. Chem. Phys.*, 2001, **115**, 402.
108. J. Schaefer, *J. Magn. Reson.*, 1999, **137**, 272.
109. T. Gullion and S. Vega, *Chem. Phys. Lett.*, 1992, **194**, 423.
110. A. E. Bennett, J. H. Ok, R. G. Griffin, and S. Vega, *J. Chem. Phys.*, 1992, **96**, 8624.
111. C. M. Rienstra, L. Tucker-Kellogg, C. P. Jaroniec, M. Hohwy, B. Reif, T. Lozano-Perez, B. Tidor, and R. G. Griffin, *Proc. Natl. Acad. Sci. U S A*, 2002, **99**, 10260.
112. A. T. Petkova, Y. Ishii, J. J. Balbach, O. N. Antzutkin, R. D. Leapman, F. Delaglio, and R. Tycko, *Proc. Natl. Acad. Sci. U S A*, 2002, **99**, 16742.
113. L. B. Andreas, A. K. Mehta, and M. A. Mehta, *J. Am. Chem. Soc.*, 2007, **129**, 15233.
114. E. Gavuzzo, F. Mazza, G. Pochetti, and A. Scatturin, *Int. J. Pept. Protein Res.*, 1989, **34**, 409.
115. C. P. Jaroniec, J. C. Lansing, B. A. Tounge, M. Belenky, J. Herzfeld, and R. G. Griffin, *J. Am. Chem. Soc.*, 2001, **123**, 12929.
116. L. Kaustov, S. Kababya, V. Belakhov, T. Baasov, Y. Shoham, and A. Schmidt, *J. Am. Chem. Soc.*, 2003, **125**, 4662.
117. L. O. Essen, R. Siegert, W. D. Lehmann, and D. Oesterheld, *Proc. Natl. Acad. Sci. U S A*, 1998, **95**, 11673.
118. H. Belrhali, P. Nollert, A. Royant, C. Menzel, J. P. Rosenbusch, E. M. Landau, and E. Pebay-Peyroula, *Structure*, 1999, **7**, 909.
119. H. Luecke, B. Schobert, H. T. Richter, J. Cartiailler, and J. K. Lanyi, *J. Mol. Biol.*, 1999, **291**, 899.
120. E. R. H. van Eck and W. S. Veeman, *J. Magn. Reson. A*, 1994, **109**, 250.
121. A. W. Hing, S. Vega, and J. Schaefer, *J. Magn. Reson. A*, 1993, **103**, 151.
122. L. Chen, R. A. Olsen, D. W. Elliott, J. M. Boettcher, D. H. Zhou, C. M. Rienstra, and L. J. Mueller, *J. Am. Chem. Soc.*, 2006, **128**, 9992.
123. K. T. Mueller, *J. Magn. Reson. A*, 1995, **113**, 81.

124. C. P. Jaroniec, C. E. MacPhee, N. S. Astrof, C. M. Dobson, and R. G. Griffin, *Proc. Natl. Acad. Sci. U S A*, 2002, **99**, 16748.
125. C. P. Jaroniec, C. E. MacPhee, V. S. Bajaj, M. T. McMahon, C. M. Dobson, and R. G. Griffin, *Proc. Natl. Acad. Sci. U S A*, 2004, **101**, 711.
126. D. M. LeMaster and D. M. Kushlan, *J. Am. Chem. Soc.*, 1996, **118**, 9255.
127. F. Castellani, B. van Rossum, A. Diehl, M. Schubert, K. Rehbein, and H. Oschkinat, *Nature*, 2002, **420**, 98.
128. A. J. Nieuwkoop, B. J. Wylie, W. T. Franks, G. J. Shah, and C. M. Rienstra, *J. Chem. Phys.*, 2009, submitted.
129. T. Gallagher, P. Alexander, P. Bryan, and G. L. Gilliland, *Biochemistry*, 1994, **33**, 4721.

### Acknowledgments

I would like to thank V. S. Bajaj, C. Filip, R. G. Griffin, J. J. Helmus, J. Herzfeld, M. Hohwy, V. Ladizhansky, J. C. Lansing, P. S. Nadaud,

B. Reif, C. M. Rienstra, and B. A. Tounge for stimulating discussions and their contributions to the development of the NMR techniques discussed here, and C. M. Rienstra for providing a copy of a manuscript prior to publication.

### Biographical Sketch

Christopher P. Jaroniec. *b.* 1974. B. S. Chemistry, Kent State University, 1997; Ph. D. Physical Chemistry, Massachusetts Institute of Technology (with R. G. Griffin), 2003; Postdoctoral Fellow, Laboratory of Chemical Physics, NIDDK, National Institutes of Health (with A. Bax), 2003–2006. Assistant Professor of Chemistry, The Ohio State University, 2006–present. Approximately 35 publications. Research interests: development of new solid-state NMR methods, applications of multidimensional solid-state NMR techniques to the studies of structure, dynamics and interactions of biological macromolecules.